

Aryl hydrocarbon receptor modulation by tuberculosis drugs impairs host defense and treatment outcomes

Andreas Puyskens¹, Anne Stinn^{1,2}, Michiel van der Vaart³, Annika Kreuchwig⁴, Jonas Protze⁴, Gang Pei⁵, Marion Klemm¹, Ute Gühlich-Bornhof¹, Robert Hurwitz⁶, Gopinath Krishnamoorthy¹, Marcel Schaaf³, Gerd Krause⁴, Annemarie H. Meijer³, Stefan H. E. Kaufmann^{*,1,7,9}, Pedro Moura-Alves^{*,1,8,9,10}

Affiliations:

¹Department of Immunology, Max Planck Institute for Infection Biology, Charitéplatz 1, 10117 Berlin, Germany.

²Department for Structural Infection Biology, Center for Structural Systems Biology, Notkestraße 85, 22607 Hamburg, Germany.

³Institute of Biology, Leiden University, Sylviusweg 72, 2333 BE Leiden, The Netherlands.

⁴Leibniz-Forschungsinstitut für Molekulare Pharmakologie, Robert-Rössle-Strasse 10, 13125 Berlin, Germany.

⁵Institute of Immunology, Friedrich Loeffler Institute, Südufer 10, 17493 Greifswald - Insel Riems, Germany.

⁶Protein Purification Core Facility, Max Planck Institute for Infection Biology, Charitéplatz 1, 10117 Berlin, Germany.

⁷Hagler Institute for Advanced Study at Texas A&M University, College Station, TX 7843, USA.

⁸Ludwig Institute for Cancer Research, Nuffield Department of Clinical Medicine, University of Oxford, OX3 7DQ, Oxford, UK.

⁹These authors share senior authorship.

*Correspondence to kaufmann@mpiib-berlin.mpg.de

*,¹⁰Lead contact & co-correspondence to pedro.mouraalves@ludwig.ox.ac.uk

Summary

Antimicrobial resistance in tuberculosis (TB) is a public health threat of global dimension, worsened by increasing drug resistance. Host-directed therapy (HDT) is an emerging concept currently explored as adjunct therapeutic strategy for TB. One potential host target is ligand-activated transcription factor aryl hydrocarbon receptor (AhR), which binds TB virulence factors and controls antibacterial responses. Here, we demonstrate that in the context of therapy, AhR binds several TB drugs, including front line drugs rifampicin (RIF) and rifabutin (RFB), resulting in altered host defense and drug metabolism. AhR sensing of TB drugs modulates host defense mechanisms, notably impairs phagocytosis and increases TB drug metabolism. Targeting AhR *in vivo* with a small molecule inhibitor increases RFB treatment efficacy. Thus, AhR markedly impacts TB outcome by affecting both host defense and drug metabolism. As a corollary, we propose AhR as a potential target for HDT in TB in adjunct to canonical chemotherapy.

Introduction

The AhR is an evolutionary highly conserved ligand-dependent transcription factor that functions as cellular sensor of both extrinsic and intrinsic chemical signals (Kawajiri and Fujii-Kuriyama, 2016). AhR ligands are diverse and encompass environmental toxins, cell- and microbe-derived metabolites and dietary products (Hubbard, Murray and Perdew, 2015). Ligand binding to AhR, induces transcription of target genes involved in xenobiotic metabolism, cell homeostasis, embryonic development, as well as immunity (Gutiérrez-Vázquez and Quintana, 2018). Previously, our group described AhR sensing of the naphthoquinone phthiocol (Pht) produced by *Mycobacterium tuberculosis* (*Mtb*), the causative agent of TB in humans, and its importance in

host defense against *Mtb* (Moura-Alves *et al.*, 2014). TB remains the leading cause of death by a single infectious agent and the emergence of antimicrobial resistance (AMR) in TB has led to a public health crisis (World Health Organization, 2019). Non-compliance and incorrect use of TB drugs have contributed to the emergence of multidrug-resistant (MDR) and extensively drug resistant (XDR) *Mtb* strains rendering several first-line drugs ineffective. AMR requires prolonged and more expensive chemotherapy regimens often with severe adverse events for patients and also constitutes an enormous economic burden (World Health Organization, 2019). To counteract AMR, HDT is an emerging concept currently explored as adjunct strategy for TB treatment (Kolloli and Subbian, 2017; Kaufmann *et al.*, 2018). Given that AhR is positioned at the center of xenobiotic metabolism regulation and host defense, AhR represents a promising target for HDT in TB. Here, we explored whether AhR not only modulates infection (Moura-Alves *et al.*, 2014), but also drug therapy. We demonstrate that (i) AhR binds and senses several first- and second-line TB drugs; (ii) AhR modulation by TB drugs inhibits macrophage phagocytosis; (iii) AhR is involved in the metabolism of RFB; (iv) inhibition of AhR by a specific small molecule inhibitor enhances RFB-mediated antimicrobial activity. Hence, we propose AhR as a candidate target for future HDT in adjunct to canonical TB drug treatment.

Results

TB drugs modulate AhR signaling. Using a previously established macrophage AhR luciferase reporter system (THP-1 AhR reporter; Moura-Alves *et al.*, 2014), we tested diverse TB drugs in clinical use for their potential to modulate AhR signaling. Of note, TB drug concentrations used in our study conform with drug concentrations used in another large European study testing different animal models (PreDiCT-TB) (Kaufmann, Rubin and Zumla, 2015). Several TB drugs modulated

AhR in reporter cells, similar to the known AhR activators 2,3,7,8-Tetrachlorodibenzo-*p*-dioxin (TCDD; Nebert, Goujon and Gielen, 1972) and the *Mtb*-derived pigment Pht (Moura-Alves *et al.*, 2014) (Figure 1A, B,C and Figure S1A,B). Among the tested first-line TB drugs (Group 1), we identified RFB as potent activator of AhR (Figure 1A, Figure S1C). Stimulation with RFB, or its major metabolite 25-O-deacetylrifabutin (25-O-DRFB), resulted in dose-dependent AhR activation (Figure S1C). Among newly approved drugs for the treatment of drug-resistant TB (Groups 2, 3, 4 and 5), we identified bedaquiline (BDQ) and linezolid (LZD) as activators of AhR (Figure S1D,E). Exposure to the specific synthetic AhR inhibitor CH-223191 (Kim *et al.*, 2006) blocked the induction of luciferase activity upon stimulation with TCDD and Pht (Figure S1F,G) as well as upon stimulation with RFB, BDQ and LZD (Figure S1H-J). Consistently, AhR knockdown showed a similar phenotype (Figure S1K-M). Several TB drugs did not activate AhR, but significantly decreased Pht-induced AhR activation when administered prior to stimulation with Pht (Figure 1B,C and Figure S1N-S). Pre-incubation with the first-line TB drugs RIF and rifapentine (RPT) markedly decreased Pht-induced AhR activation (Figure 1B,C and Figure S1N). Similarly, stimulation with TB drugs of groups 3, 4 and 5 including enrofloxacin (ERF), moxifloxacin (MXF), ethionamide (ETA), clofazimine (CFZ) and thiacetazone (THZ) also decreased Pht-induced AhR activation (Figure S1O-S). Taken together, using a macrophage AhR luciferase reporter system, we identified several first- and second-line TB drugs as potent modulators of the canonical AhR pathway (Table 1).

Both RFB and RIF are key first-line TB drugs (World Health Organization, 2016). Based on the observed opposing effects on AhR modulation, we further focused on the characterization of RFB- and RIF-mediated effects on AhR, as examples of TB drugs with AhR modulatory capacities. To exclude that AhR modulation mediated by RFB and RIF was due to impaired cell viability, we

monitored lactate dehydrogenase release (LDH) and caspase-3/7 activity of reporter macrophages. No significant differences were observed under the conditions tested (Figure S2A,B). Similar to Pht, RFB induced the expression of AhR-dependent genes (*CYP1A1*, *CYP1B1*, *AHRR*) in THP-1 macrophages, whereas *AHR* expression itself remained unaltered (Figure 1D and Figure S2C). Consistently, in a murine hepatocyte cell line (Hepa-1c1c7) RFB activated AhR in a dose-dependent manner (Figure S2D). Recently, it was reported that AhR activity can be modulated indirectly via dysregulation of CYP1A1 (Wincent *et al.*, 2012). To evaluate whether inhibition of CYP1A1 by RFB activates AhR indirectly, we measured CYP1A1 enzymatic activity. Stimulation of Hepa-1c1c7 cells with RFB led to a dose-dependent increase in enzymatic CYP1A1 activity, similar to stimulation with Pht or TCDD (Figure 1E,F). Thus, we exclude indirect AhR activation by CYP1A1 inhibition. In contrast, RIF stimulation of Hepa-1c1c7 cells did not induce CYP1A1 activity, but profoundly inhibited Pht-induced CYP1A1 activity (Figure 1G,H). Our data suggest that both RFB and RIF are modulators of the canonical AhR pathway with opposing effects on AhR signaling.

RFB and RIF bind to AhR. To evaluate binding of TB drugs to AhR, we tested ligand binding to a purified AhR protein by microscale thermophoresis (MST). MST allows measurement of protein-ligand interactions based on temperature-induced changes in fluorescence of a target of interest (here AhR) and a non-fluorescent ligand (Seidel *et al.*, 2013). We confirmed binding of RIF (K_d 11.3 μ M), RFB (K_d 16.1 μ M) as well as the RFB metabolite 25-O-DRFB (approximate K_d 24.5 μ M) to AhR (Figure 2A-C and Figure S3A,B). Importantly, binding to the AhR nuclear translocator (Arnt) was not observed, indicating the specificity of ligand binding to AhR under the conditions tested. As control, we tested binding of isoniazid (INH), another first-line TB drug, for which we observed no AhR modulation in the reporter assay (Table 1). Consistently, we did not

detect binding of INH to AhR (Figure S3A,C). We conclude that the first-line TB drugs RIF and RFB, as well as its metabolite 25-O-DRFB, bind to and modulate AhR activity, rendering antimycobacterial drugs a class of AhR ligands.

The atomic structure of the AhR ligand binding domain remains unknown. Therefore, despite being only predictive, computational based molecular modeling studies are widely used to predict how different ligands bind to and modulate AhR functions (Pohjanvirta, 2011; Moura-Alves *et al.*, 2014; Corrada, Denison and Bonati, 2017; Mahiout *et al.*, 2018). We applied molecular modeling and *in silico* docking to determine how RFB and RIF fit into the proposed binding pocket of AhR (Moura-Alves *et al.*, 2014). Despite structural similarities of the cyclic part between RFB and RIF, parts of their backbone conformations, orientations and size of the substituents differ (Figure 2C). Although RFB and RIF do not resemble prototypic AhR ligands (Figure 2C and Figure S3D) molecular modeling and *in silico* docking resulted in putative fitting into the ligand binding pocket of the AhR-PasB model, with only few possible configurations (calculated ΔG binding: RFB= -130.16 kcal/mol, RIF= -125.21 kcal/mol and -118.66 kcal/mol, Table S1). Interestingly, docking of RFB and RIF into the AhR binding pocket resulted in different orientations, suggesting dissimilar interaction profiles (Figure 2D and Table S1). Within the AhR-PasB ligand binding pocket, RFB formed multiple hydrogen bonds with the side chains of Thr289, His291, Ser365 and Gln383, altering the existing H-bond network between these residues. Such rearrangements influence the structural adjustment, especially the N- and C-terminal endings of particular β -strands (segments A, I, J) of the β -sheet and the AB-loop, which leads to a constrained backbone conformation at two locations. First, at the AB-loop as part of the interface between AhR and PasB of Arnt (Corrada, Denison and Bonati, 2017; Corrada *et al.*, 2016), comprised of Phe295 (AB-loop), Tyr322 (helix E) and His337 (helix F; Figure 2D, Figure S3E,F). Second, at the interface

between AhR and the PasA of Arnt (Figure S3E) that is formed by outward oriented residues on the N-terminal end of β -strand A (Ile286) and/or on the backside of β -strands I, J (Gln364 and Arg384; Figure 2D). Compared to RFB, both RIF and the specific AhR inhibitor CH-223191 (Figure 2D; Figure S3D,F and Table S1), formed considerably less H-bonds to residues on the β -strands A, I and J. Such differences in RFB, RIF and CH-223191 binding to AhR lead to opposing conformational influence on the two interaction positions, potentially impacting AhR activation.

Modulation of AhR impairs macrophage phagocytosis. We further evaluated potential effects of ligand-induced AhR modulation in the context of infection and TB drug therapy. We assessed whether AhR could play a role in macrophage phagocytosis of *Mtb*. Inhibition of AhR by CH-223191 in THP-1 macrophages reduced the uptake of *Mtb* H37Rv (Figure 3A). Likewise, AhR-inhibition decreased uptake of fluorescently-labelled *Mtb* H37Rv, paralleled by a reduction in the proportion of *Mtb*-harboring cells (Figure 3B,C and Figure S4A). Exposure to CH-223191 did not affect *Mtb* or macrophage viability (Figure S4B-F). Consistently, knockdown of AhR in THP-1 macrophages likewise resulted in reduced uptake of *Mtb* H37Rv (Figure 3D). To further characterize the role of AhR in phagocytosis, we used the fungal glucan zymosan conjugated to a pH-sensitive dye (pHrodo), which allows visualization of phagosomal uptake and acidification (Queval *et al.*, 2017). Consistent with *Mtb* phagocytosis, the proportion of zymosan-containing macrophages and the rate of internalization were decreased upon AhR inhibition (Figure 3E,F). AhR inhibition also reduced pHrodo fluorescence intensity of internalized zymosan, indicating AhR-dependent impact on macrophage phagosomal acidification (Figure 3G). Our data suggest a role for AhR in macrophage phagocytosis of *Mtb* and the fungal glucan zymosan.

We extended our investigation of AhR-dependent phagocytosis to other AhR ligands, including TB drugs. The AhR antagonist RIF, potently inhibited uptake of zymosan-pHrodo by macrophages,

as indicated by reduced numbers of zymosan-containing cells and rate of internalization (Figure 3H,I). Moreover, RIF impaired phagosomal acidification, similar to the synthetic AhR inhibitor (Figure 3G, J). Notably, a similar phenotype was observed upon exposure to the AhR agonists TCDD and RFB (Figure 3K-M). In contrast, INH, which neither binds nor modulates AhR, did not impair phagocytosis (Figure S4G-I). To further explore RIF elicited effects on the AhR, in the absence of a direct antimicrobial effect on *Mtb*, we took advantage of a RIF-resistant *Mtb* strain. Similar to what we observed for zymosan-pHrodo, RIF treatment of macrophages reduced uptake of the RIF-resistant patient isolate (Figure 3N). RIF-resistance was confirmed by monitoring cultural growth in the presence or absence of RIF, in comparison to a drug-sensitive *Mtb* patient isolate (Figure S4J,K) as well as by next generation sequencing and drug susceptibility testing (Table S2). We conclude that ligand-induced AhR modulation impairs macrophage phagocytosis. Moreover, we identified a yet unknown host-directed effect of the TB drugs RIF and RFB on macrophage phagocytosis.

AhR is involved in metabolism of RFB. Pharmacokinetic and -dynamic factors markedly influence drug availability and efficacy, essential for successful treatment (Rowland and Tozer, 2011). AhR is a central regulator of xenobiotic metabolism (Stockinger *et al.*, 2014). Hence, we evaluated whether AhR is involved in the metabolism of RFB. To this end, we made use of the human hepatic stem cell line HepaRG, whose AhR expression levels have been reported to be comparable to primary human hepatocytes (Guillouzo *et al.*, 2007). Moreover, HepaRG cells express multiple functional phase 1 and 2 drug metabolizing enzymes, rendering them suitable for studies on xenobiotic metabolism (Guillouzo *et al.*, 2007). We monitored RFB clearance from cell culture supernatants using ultra performance liquid chromatography (UPLC). We observed continuous elimination of RFB from HepaRG cell cultures (Figure 4A). Strikingly, RFB recovery

from supernatants of AhR-inhibited cells was higher, when compared to solvent controls (Figure 4B). Importantly, treatment of HepaRG cells with CH-223191 and/or RFB did not impair cell viability at the concentrations used (Figure S5A,B). Our data suggest that AhR is involved in hepatic metabolism of RFB and that inhibiting AhR reduces RFB metabolism, ultimately affecting its availability.

***In vivo* modulation of AhR by TB drugs.** The zebrafish (*Danio rerio*) has emerged as valuable animal model to study toxicology (Roper and Tanguay, 2018) and mechanisms of disease, including TB (Van Leeuwen, Van Der Sar and Bitter, 2015). Increasingly, zebrafish have been harnessed for high-throughput *in vivo* screenings of novel drug candidates, such as antimicrobials (Zhong and Lin, 2011; Dalton *et al.*, 2017). We used zebrafish to validate our *in vitro* findings. Similar to what we observed in cell lines, exposure of zebrafish embryos to RFB induced AhR-downstream target genes, such as *ahrta* (Evans *et al.*, 2005), *ahrrb* (Evans *et al.*, 2005) and *cyp1a* (Prasch *et al.*, 2003), in an AhR-dependent manner (Figure 5A). Furthermore, *in vivo* EROD assays detected increased Cyp1a enzymatic activity upon RFB exposure, similar to that induced by Pht (Figure 5B). CH-223191 blocked *cyp1a* gene expression (Figure 5A) and induction of Cyp1a enzymatic activity (Figure 5C). Exposure of zebrafish embryos to increasing concentrations of RIF did not induce Cyp1a activity (Figure 5D), instead RIF potentially inhibited TCDD-induced Cyp1a enzymatic activity (Figure 5E). We did not detect toxicity in zebrafish for any of the ligands and conditions tested (Figure S6A,B). To evaluate whether AhR also plays a role in RFB metabolism *in vivo*, we exposed zebrafish embryos to RFB in the water and collected samples at 4 d post exposure. In agreement with results from human hepatocyte cultures (Figure 4B), AhR inhibition in zebrafish resulted in higher RFB recovery as compared to controls (Figure 5F). Altogether, we demonstrate that *in vivo* exposure of zebrafish embryos to TB drugs, such as RFB and RIF,

modulate AhR downstream responses, including regulation of gene expression and drug metabolism.

Modulation of AhR during mycobacterial infection and treatment *in vivo*. We interrogated whether AhR-dependent RFB degradation affects the efficacy of drug treatment *in vivo*. To this end, we made use of the zebrafish-*Mycobacterium marinum* infection model, of mycobacterial pathogenesis (Van Leeuwen, Van Der Sar and Bitter, 2015). Stimulation of AhR reporter macrophages with filtered *M. marinum* culture supernatants induced AhR activation (Figure S7A), similar to *Mtb* and *Mycobacterium bovis* Bacillus Calmette–Guérin (BCG; Moura-Alves *et al.*, 2014). Exposure of zebrafish embryos to *M. marinum* by immersion, as a natural route of infection (Dalton *et al.*, 2017), induced Cyp1a enzymatic activity in zebrafish embryos, as did TCDD (Figure 6A and Figure S7B). Cyp1a enzymatic activation was abrogated by CH-223191 (Figure 6A). Our data support previous findings in other models, including mouse, that mycobacterial infection activates AhR signaling (Moura-Alves *et al.*, 2014). Hence, zebrafish represent a suitable *in vivo* model to study the role of AhR during infection and drug treatment.

Intravenous infection of zebrafish embryos with *M. marinum* followed by AhR inhibition (CH-223191), resulted in higher bacterial burden in embryos, as compared to controls (Figure 6B,C). This is in line with the increased bacterial burden observed in AhR knockout mice infected with *Mtb* (Moura-Alves *et al.*, 2014). Importantly, we did not identify any direct effect of the specific AhR-inhibitor CH-223191 on bacterial growth or fluorescence (Figure S8A-C), nor did we observe adjuvant effects of CH-223191 during RFB treatment (Figure S8D,E). Interestingly and in agreement with our *in vitro* results, we observed a delay in macrophage phagocytosis of *M. marinum* upon CH-223191 treatment in zebrafish embryos *in vivo* (Figure S8F,G). Based on our results suggesting a role for AhR in RFB metabolism, we evaluated whether inhibition of AhR in

228 *M. marinum*-infected zebrafish embryos affects efficacy of RFB treatment. Treatment with RFB
229 dose-dependently decreased bacterial loads (Figure 6B,C), confirming antimicrobial activity of
230 RFB in *M. marinum*-infected zebrafish embryos. Remarkably, AhR inhibition by CH-223191
231 enhanced RFB-mediated bacterial killing compared to AhR-proficient controls (Figure 6B,C)
232 correlating with higher drug concentrations upon AhR inhibition (Figure 4B and Figure 5F). Of
233 note, we did not observe AhR-dependent difference in bacterial killing upon RIF treatment in
234 zebrafish embryos and did also not observed changes in RIF metabolism upon AhR inhibition
235 (Figure S8H,I). Taken together, our data unveil that AhR concomitantly senses infection and drug
236 treatment, thereby playing a central role in host-pathogen interactions and treatment in TB.

237

Discussion

Here, we demonstrate that differential modulation of AhR by TB drugs influences both host defense and treatment outcome. Hence, AhR is a critical denominator in TB. More precisely, we demonstrate that: (i) TB drugs, including the first-line drugs RFB and RIF, are AhR ligands; (ii) AhR modulation by both RFB and RIF impair macrophage phagocytosis and phagosomal acidification; (iii) RFB and RIF differentially regulate AhR target gene expression and enzymatic Cyp1a activity *in vitro* and in zebrafish; (iv) inhibition of AhR impairs metabolism of RFB in human hepatocytes and in zebrafish; (v) pharmacological inhibition of AhR augments RFB-mediated antimicrobial activity in *M. marinum*-infected zebrafish embryos.

After aerogenic infection, macrophages are amongst the first host cells to encounter *Mtb* (Gengenbacher and Kaufmann, 2012). We demonstrate that inhibition of AhR affects phagocytosis of both *Mtb* and zymosan, by a currently unknown mechanism. Previous studies showed an involvement of AhR in actin polymerization and cytoskeleton remodeling (Carvajal-Gonzalez *et al.*, 2009; Angeles-Floriano *et al.*, 2016). Thus, it is tempting to speculate that AhR-mediated regulation of this process can potentially impact phagocytosis, although further studies are needed to evaluate this hypothesis. Our findings are reminiscent of a recent study reporting that AhR activation by the opportunistic pathogenic yeast *Candida albicans* promotes endocytosis by epithelial cells and that AhR inhibition reduces fungal invasion (Solis *et al.*, 2017). Consistently, exposure to the AhR ligands RFB and RIF likewise reduced macrophage phagocytosis. Our observations are in agreement with earlier studies reporting effects of antibiotics on macrophage phagocytosis (Nishida *et al.*, 1976; Bode *et al.*, 2014). We conclude that impaired phagocytosis by TB drugs impacts on host defense and thereby influences therapy outcome. Due to the vast spectrum of modulatory AhR ligands, this mechanism should be taken into consideration for: (i)

antibiotic treatment of bacterial infections, in which phagocytosis plays a critical role, such as TB, and (ii) drug treatment in presence of environmental AhR modulators, which could affect host defense and drug availability. Environmental risk factors for AhR modulation may set a basal threshold, which affects diverse pathophysiological pathways. For example, cigarette smoke contains several potent AhR agonists, including TCDD (Muto and Takizawa, 1989) and benzo(a)pyrene (Stedman, 1968). AhR has been shown to regulate cigarette smoke-induced cyclooxygenase-2 (COX-2) and prostaglandin E₂ (PGE₂; Martey *et al.*, 2005) expression, the latter being critical in immunopathogenesis of TB (Rangel Moreno *et al.*, 2002). It is therefore tempting to envision that AhR signaling could participate in the heightened risk of smokers for TB (Alcaide *et al.*, 1996) and in their poor therapy outcome (Leung *et al.*, 2015; Yen *et al.*, 2014).

The currently recommended treatment regimen of patients with drug-susceptible TB consists of at least four drugs given over an extended period of time (2 month intensive treatment with INH, RIF, PZA, EMB, followed by 4 month continuation treatment with INH and RIF; World Health Organization, 2017). We identified TB drugs, which modulate the AhR pathway in opposite ways, including RFB and RIF that activated or inhibited AhR, respectively. In combination therapy, this could result in synergistic or antagonistic effects and hence should be taken into consideration when formulating novel multidrug treatment regimens for TB. The emergence of MDR- and XDR-TB has become a global public health threat (World Health Organization, 2019). Treatment duration (Olofsson and Cars, 2007) and suboptimal drug concentrations (DeRyke *et al.*, 2006; Mitchison, 1998) promote the development of AMR. Drug metabolism influences duration and intensity of pharmacological action and is therefore considered critical for AMR selection (Baquero *et al.*, 1997; Negri *et al.*, 2000). Here, targeting AhR by a specific small molecule inhibitor reduced the metabolism of RFB resulting in elevated drug concentrations and increased

RFB-mediated antimicrobial activity. We conclude that modulation of AhR affects overall drug availability and potentially the development of AMR. Identification of suitable HDT targets is of vital importance to counteract the rising threat posed by AMR in TB. Given the central role of AhR in infection and treatment, we propose AhR as candidate target for adjunct HDT in TB. Of note, targeting AhR has already been harnessed in other disease models (Yeste *et al.*, 2012, 2016; Zelante *et al.*, 2013; Parks *et al.*, 2014; Cervantes-Barragan *et al.*, 2017; Smith *et al.*, 2017; Lozza *et al.*, 2019). Although, due to its vast ligand binding capacity (e.g. allowing sensing of both bacteria and drug treatment), as well as its implication in multiple cellular and tissue mechanisms, targeting the AhR might carry potential risks that need to be further evaluated. The work herein presented serve as the foundation for future studies to ultimately verify the suitability of the AhR as HDT in TB, looking at both potential benefits and risks of such therapeutic intervention.

Acknowledgements

The authors acknowledge those, who have provided tools and materials for this study. Expression plasmid pET30-EK/LIC-Arnt was a gift from Oliver Daumke and Kathrin Schulte (Max Delbruck Center, Berlin, Germany). Stefan Niemann, Katharina Kranzer and Anne Witt (Forschungszentrum Borstel, Borstel, Germany) kindly provided and characterized *Mtb* patient isolates. Christiane Guguen-Guillouzo, Philippe Gripon and Christian Trepo kindly made available the HepaRG cell line. Clemens Grabher (Karlsruhe Institute of Technology, Karlsruhe, Germany) and Daniela Panakova (Max Delbruck Center, Berlin, Germany) provided zebrafish AB WT strain. We acknowledge Norman Fielko, Jens Otto, Andrey Fadeev (Max Planck Institute for Infection Biology, Berlin, Germany), as well as Mariana Simões (Max Delbruck Center, Berlin, Germany) for zebrafish breedings.

This work was generously supported by SPP 1937 (DFG Project KA 573/6-1 (SPP 1937) and an internal grant of the Max Planck Society to SHEK and by the International Max Planck Research School for Infectious Diseases and Immunology (IMPRS-IDI) to AP and AS.

Author contributions

Conceptualization, AP, SHEK and PM-A; Methodology, AP, AS, SHEK, MvV, MS, AHM, AK, GK, JP, PM-A; Formal Analysis, AP, SHEK, MvV, AK, GK, JP and PM-A; Investigation, AP, AS, GP, GK, UT, MT, MvV, RH, AK, GK, JP and PM-A; Funding Acquisition: AP, AS and SHEK; Writing – Original Draft, AP, SHEK and PM-A; Writing – Review & Editing, AP, SHEK and PM-A; Visualization, AP and PM-A; Supervision, AHM, GK, SHEK and PM-A.

Declaration of interests

The authors declare no competing interests. Correspondence and requests for materials to SHEK (corresponding author) or PM-A (co-corresponding author).

Main figure titles and legends

Figure 1- RFB and RIF modulate AhR signaling *in vitro*. (A,B,C) Luciferase activity of macrophage (THP-1) luciferase AhR reporter cells upon (A, B) 4 h stimulation with RFB, RIF or Pht. (C) Pht-RIF competition assay: first pre-incubation with increasing concentrations of RIF for 1 h, followed by 3 h stimulation together with 50 μ M Pht, or Pht alone as control. (D) Gene expression analysis of AhR-dependent genes in THP-1 macrophages upon stimulation with Pht or RFB for 4 h. (E,F) Hepatic CYP1A1 enzymatic activity (Hepa-1c1c7) upon stimulation with increasing concentrations of RFB and (E) TCDD over time or (F) Pht after 24 h. (G,H) Hepatic CYP1A1 enzymatic activity (Hepa-1c1c7) upon stimulation with (G) Pht or increasing concentrations of RIF. (H) Pht-RIF competition assay: first pre-incubation with increasing concentrations of RIF for 1 h, followed by stimulation together with 50 μ M Pht or Pht alone for 3 h. (A-C,F) 1 representative of n=4 independent experiments. (D,E,G,H) 1 representative of n=3 independent experiments. (A-D,F-H) Mean \pm S.D. shown. (E) Mean only shown. (D) Unpaired t test. **P \leq 0.01, ***P \leq 0.001, ****P \leq 0.0001. See also Figure S1 and S2.

Figure 2- AhR binding of TB drugs. (A,B) AhR binding studies of (A) RFB and (B) RIF to the AhR protein complex (AhR-Arnt) or Arnt alone using MST. (C) Chemical structures of RFB and RIF. (D) Best scoring ligand docking poses for RFB (left, magenta) and RIF (right, yellow) in the *in silico* model of the hAhR-PasB. H-bonds are depicted as yellow dotted lines; different conformations of the outward oriented residues F295, Y322 and H337 are depicted in pale wheat; outward oriented residues on the backside of the β -sheet A, I, J (Ile286, Gln364 and Arg384) that are able to interact with PasA of Arnt are depicted in pale blue. (A,B) Median \pm S.D. of triplicates shown. See also Figure S3 and Table S1.

Figure 3- Modulation of phagocytosis by AhR. (A-D) Uptake of *Mtb* MOI of 10 by AhR proficient or deficient (12 μ M CH-223191 pre-treatment for 2 h or shRNA knockdown) THP-1 macrophages after 4 h, measured by (A,D) CFU (*Mtb* H37Rv) or (B,C) microscopy (*Mtb*-GFP H37Rv). (E-G) Phagocytosis of zymosan-pHrodo by macrophages (RAW264.7) 2 h after pre-incubation with 12 μ M CH-223191 or DMSO (solvent) for 2 h. (E) Percentage of zymosan-pHrodo positive cells, (F) rate of zymosan-pHrodo internalization, (G) average intensity of internalized pHrodo. (H-M) Phagocytosis of zymosan-pHrodo by macrophages (THP-1) 2 h after pre-incubation with (H-J) RIF and (K-M) TCDD or RFB for 2 h. (H,K) Percentage of zymosan-pHrodo positive cells, (I,L) rate of internalization of zymosan-pHrodo, (J,M) average intensity of internalized pHrodo. (N) Uptake of RIF-resistant *Mtb* MOI of 10 by THP-1 macrophages pre-treated for 2 h with 10 μ M RIF or DMSO (solvent) after 4 h, measured by CFU. (A,D) 1 representative of n=2 independent experiments. (B,C,E-M) 1 representative of n=3 independent experiments. (N) Pooled data from n=2 independent experiments. Shown as (A,D) mean \pm S.D.,

(B,C,E,H,K) box plot with Tukey whiskers, (F,G,I,J,L,M) scatter dot plot with mean, (N) mean \pm S.E.M. (A-M) Unpaired t test. * $P \leq 0.05$, ** $P \leq 0.01$, **** $P \leq 0.0001$. (N) Mann-Whitney test. * $P \leq 0.05$. See also Figure S4 and Table S2.

Figure 4- AhR inhibition in human hepatocytes affects RFB availability. (A) Percentage of RFB recovery from HepaRG culture supernatants over time compared to no cells control for each time point. (B) Percentage of RFB recovery from HepaRG culture supernatants in the presence or absence of CH-223191 after 48 h compared to the input and normalized to no cells control. (A) 1 representative of n=3 independent experiments. Mean \pm S.D shown. (B) Pooled data from n=2 independent experiments. Mean \pm S.E.M. shown. See also Figure S5.

Figure 5- AhR modulation by RFB and RIF *in vivo*. (A) Gene expression analysis of AhR-target genes in 2 dpf zebrafish embryos upon 4 h of stimulation with RFB, in the presence or absence of CH-223191. (B-E) *Cyp1a* enzymatic activity (EROD) in 2 dpf embryos treated for 4 h with (A) Pht or increasing concentrations of RFB; (C) with RFB in the presence or absence of CH-223191; (D) with TCDD or increasing concentrations of RIF; (E) with TCDD in the presence or absence of RIF. (F) Recovery of RFB from the water of zebrafish embryos after 4 d exposure to 5 μ M RFB in the presence of 10 μ M CH-223191 compared to DMSO (solvent) control. (A) Triplicates, each consisting of 12 zebrafish embryos pooled. Mean \pm S.D. shown. (B-E) Each data point depicts an individual zebrafish embryo. Mean \pm S.E.M. shown. (A-E) 1 representative of n=3 independent experiments. (F) Pooled data from n=2 independent experiments. Mean \pm S.E.M. shown. (A-F) Unpaired t test. ns (not significant), * $P \leq 0.05$, ** $P \leq 0.01$, *** $P \leq 0.001$, **** $P \leq 0.0001$. See also Figure S6.

Figure 6- AhR modulation during *M. marinum* infection and RFB treatment *in vivo*. (A) *Cyp1a* enzymatic activity (EROD) in 2 dpf embryos exposed to *M. marinum* for 24 h in E3 medium, in the presence or absence of 10 μ M CH-223191. (B,C) Bacterial loads in zebrafish embryos at 4 d post systemic infection with Wasabi-expressing *M. marinum* (200 CFU), untreated or treated with RFB for 3 d, in the presence or absence of 10 μ M CH-223191. (B) Representative micrographs. (C) Quantification of Wasabi-expressing *M. marinum* pixels per whole embryo. (A,C) Each data point depicts an individual zebrafish embryo, (C) while orange symbols indicate the individuals that were chosen as representative micrograph. (A) 1 representative of n=3 independent experiments. Mean \pm S.D. shown. (B,C) 1 representative of n=2 independent experiments. Mean \pm S.E.M. shown. (A,C) Unpaired t test. * $P \leq 0.05$, ** $P \leq 0.01$, **** $P \leq 0.0001$. See also Figure S7 and S8.

Main tables and legends

Table 1- List of TB drugs tested in the AhR reporter assay.

Group	Description	Drug	Abbreviation	AhR modulation
1	First-line oral TB drugs	Ethambutol	EMB	No effect
		Isoniazid	INH	No effect
		Pyrazinamide	PZA	No effect
		Rifabutin	RFB	Activator

		Rifampicin	RIF	Inhibitor
		Rifapentine	RPT	Inhibitor
2	Injectable TB drugs	Amikacin	AMK	No effect
		Kanamycin	KAN	No effect
		Streptomycin	STM	No effect
3	Fluoroquinolones	Enrofloxacin	ERF	Inhibitor
		Moxifloxacin	MXF	Inhibitor
4	Second-line oral TB drugs	Bedaquiline	BDQ	Activator
		Clofazimine	CFZ	Inhibitor
		Ethionamide	ETA	Inhibitor
		Linezolid	LZD	Activator
		<i>p</i> -aminosalicylic acid	PAA	No effect
5	Currently not included in core MDR-TB regimen	Thiacetazone	THZ	Inhibitor

392

393

STAR★Methods

LEAD CONTACT AND MATERIALS AVAILABILITY

Further information and requests for resources and reagents should be directed to and will be fulfilled by the Lead Contact, Pedro Moura-Alves (pedro.mouraalves@ludwig.ox.ac.uk). Plasmids generated in this study will be made available upon request. There are restrictions to the availability of HepaRG cells due to a material transfer agreement with Société Anonyme à Directoire et Conseil de Surveillance (Inserm Transfert SA).

EXPERIMENTAL MODEL AND SUBJECT DETAILS

Bacterial Strains and Maintenance. *Mycobacterium tuberculosis* (*Mtb*) H37Rv, *Mtb* H37Rv-GFP and *Mtb* patient isolates (RIF-mono-resistant isolate 18000790 or drug-sensitive isolate 18000880, Forschungszentrum Borstel, Borstel, Germany) were cultured in Middlebrook 7H9 broth (BD) supplemented with 0.05% Tween 80 (Sigma-Aldrich) and 10% albumin-dextrose-catalase (ADC, BD) at 37°C in an orbital shaking incubator at 100 rpm. *Mtb* H37Rv-GFP was kept with additional 25 µg/ml kanamycin (Sigma-Aldrich). *Mycobacterium marinum* E11 and M strains were cultured in Middlebrook 7H9 broth (BD) supplemented with 0.05% Tween 80 (Sigma-Aldrich) and 10% oleic albumin-dextrose-catalase (OADC, BD) statically at 30°C protected from exposure to light. *M. marinum* M strain expressing pTEC15-Wasabi (*M. marinum*-Wasabi; Takaki *et al.*, 2013) was kept with additional 50 µg/ml hygromycin (Sigma-Aldrich).

Cell Culture and Maintenance. THP-1 cells (CVCL_0006, human monocytes, ATCC TIB-202), THP-1 AhR reporter (Moura-Alves *et al.*, 2014) and THP-1 AhR knockdown (Moura-Alves *et al.*, 2014) cells were grown in RPMI 1640 (Gibco), supplemented with 10% (v/v) heat-inactivated fetal

416 calf serum (FCS; Gibco), 1% (v/v) sodium pyruvate (Gibco), 1% (v/v) L-glutamine (Gibco),
417 1% (v/v) non-essential amino acids (MEM NEAA, Gibco), 1% (v/v) 4-(2-hydroxyethyl)-1-
418 piperazineethanesulfonic acid (HEPES, Gibco) and 0.05 M 2-mercaptoethanol (Gibco). Hepa-
419 1c1c7 cells (CVCL_0328, mouse hepatocytes, ATCC CRL-2026) were grown in DMEM (Gibco)
420 supplemented with 10% (v/v) FCS, 1% (v/v) sodium pyruvate and 1% (v/v) L-glutamine,
421 1% (v/v) HEPES. Undifferentiated HepaRG cells (human hepatic progenitors, HPR101) were
422 cultured in 710 growth medium containing antibiotics and differentiated using 720 differentiation
423 medium containing antibiotics (all Biopredic International). AhR reporter cells were generated in
424 accordance with the protocols available at the Genetic Perturbation Platform (GPP) of the Broad
425 Institute (<https://portals.broadinstitute.org/gpp/public/>) as described previously (Moura-Alves *et*
426 *al.*, 2014). In particular, a replication incompetent VSV-g pseudotyped lentivirus expressing the
427 firefly luciferase gene under transcriptional control of a minimal CMV promoter and tandem
428 repeats of the XRE (Cignal Lenti XRE Reporter) was used for infection of THP-1 cells. A similar
429 protocol was used for the generation of AhR knockdown cells. Reporter cells and knockdown cells
430 were kept with additional 5 µg/ml puromycin (Calbiochem). THP-1 monocytes were differentiated
431 into macrophages by treatment with 200 nM of phorbol 12-myristate 13-acetate (PMA, Sigma-
432 Aldrich) for 4 d and rested in plain medium for another 4 d before further experiments. For
433 CYP1A1 enzymatic activity measurements (EROD; Mohammadi-Bardbori and Mohammadi-
434 Bardbori, 2014), Hepa-1c1c7 cells were kept in DMEM medium without phenol red (Gibco).
435 HepaRG cells were cultured in 710 growth medium for 2 weeks and subsequently differentiated
436 by switching to 720 differentiation medium for another 2 weeks prior to experiments according to
437 the protocols by Biopredic International. All cells were kept in a humidified incubator (Heratherm,
438 Thermo Fisher Scientific) at 37°C with 5% CO₂. Sex of the cell lines was not a consideration in
439 this study. Cell lines were obtained from authentic stocks (ATCC and Biopredic International). If

not specified otherwise in the figure legend, the highest concentration of DMSO used in the experiments did not exceed 1%.

Zebrafish model. All zebrafish (*Danio rerio*) husbandry and experimental procedures adhered to the international guidelines specified by the EU Animal Protection Directive 2010/63/EU and experiments were approved by, and conducted in accordance with the guidelines of the Landesamt für Gesundheit und Soziales (LaGeSo, Berlin, Germany) and the animal welfare committee of the Max Planck Institute for Infection Biology (MPIIB, Berlin, Germany). Only wildtype AB strain zebrafish (ZDB-GENO-960809-7) were used in this study. Adult zebrafish used to generate embryos were housed in 3.5 L or 8 L tanks (Tecniplast) under the following water conditions: 28°C; conductivity ~500 µS (using Instant Ocean Sea Salt); pH 7.4-7.5. Zebrafish embryos were raised and maintained according to standard protocols (<http://zfin.org>). All zebrafish embryos used in this study were euthanized on or before 5 dpf. At these ages, sex is indeterminate (Uchida *et al.*, 2002; Liew and Orban, 2014), hence no distinction between male and female was made.

Zebrafish embryos were maintained in E3 medium (5 mM NaCl, 0.17 mM KCl, 0.33 mM CaCl₂, 0.33 mM MgSO₄; Nüsslein-Volhard and Dahm, 2002) incubated at 28.5°C in petri dishes at a maximum density of 50 embryos per dish. To suppress fungal growth, methylene blue (2 ml of 0.1% methylene blue in 1l E3 medium) was added in experiments that did not involve microscopy. Embryos were manually dechorionated at 1 dpf aided by a stereomicroscope (MZ6, Leica). Prior to experimental manipulations, zebrafish embryos were anesthetized using buffered 3-aminobenzoic acid (Tricaine, MS-222, Sigma-Aldrich) at a final concentration of 200 µg/ml. For experiments, embryos were pooled and randomly allocated to experimental groups. At the end of experiments, embryos were euthanized using an overdose of 300 mg/l Tricaine (Sigma-Aldrich).

METHOD DETAILS

Gene Expression Analysis by qRT-PCR. For the isolation of total RNA from cells, buffer RLT (Qiagen) containing 1% 2-Mercaptoethanol (Sigma-Aldrich) was used. For the isolation of total RNA from zebrafish embryos TRIzol (Invitrogen) was used. RNA extraction was performed using RNeasy Plus Mini kit (Qiagen) according to the manufacturer's instructions. RNA quality and concentration were determined by spectrophotometry (Nanodrop 2000c, Thermo Fisher Scientific). Complementary DNA (cDNA) was generated using iScript cDNA synthesis kit (Biorad) according to the manufacturer's instructions. Quantitative real time polymerase chain reaction (qRT-PCR) was performed using Power SYBR green (Thermo Fisher Scientific) in a LightCycler® 480 II PCR platform (Roche) running with LightCycler® 480 Software (SCR_012155, Version 1.5.1, Roche). The average threshold cycle of triplicate reactions was applied for all calculations and $\Delta\Delta C_t$ method was used (Pfaffl, 2001). Gene expression was normalized to glyceraldehyde-3-phosphate dehydrogenase (*GAPDH*) or β -actin for human and zebrafish samples, respectively. qRT-PCR data were generated from independent experiments, with at least 3 biological replicates per experiment. Sequences of all primers used are listed in Table S3.

Luciferase Reporter Assay. AhR reporter cells were stimulated as depicted in figure legends. For competition assays, AhR reporter cells were pre-incubated with TB drugs for 1 h prior to stimulation with 50 μ M Pht. After stimulation, cells were washed using sterile Dulbecco's phosphate-buffered saline (DPBS, Gibco) and subsequently lysed using 1x concentrated Reporter Lysis Buffer (Promega). Cell lysates were used to determine luciferase activity by Luciferase Assay System (Promega) according to the manufacturer's instructions and luminescence was measured with an Infinite M200 pro reader platform (TECAN). Luciferase activity was normalized to the protein concentration measured by Bradford reaction (PierceTM Coomassie Plus Assay, Thermo

Fisher Scientific). Results are shown as log₂ fold induction normalized to the solvent control of the respective time point.

siRNA knockdown of AhR. THP-1 AhR reporter cells were treated with ON-TARGET plus siRNA AHR or ON-TARGETplus Non-targeting Pool (Dharmacon) for 24 h prior to stimulation with RFB, according to manufacturer's instructions.

EROD Activity *in vitro*. *CYP1A1* is under transcriptional control of AhR (Nebert, Goujon and Gielen, 1972; Poland, Glover and Kende, 1976; Poland and Knutson, 1982). The EROD assay measures the conversion of non-fluorescent ethoxyresorufin by CYP1A1 to the fluorescent product resorufin, where the amount of resorufin-fluorescence is proportional to the enzymatic activity of CYP1A1 (Mohammadi-Bardbori and Mohammadi-Bardbori, 2014). Cells were stimulated as depicted in the figures. After stimulation, cells were washed once using sterile DPBS (Gibco) and 5 µM ethoxyresorufin (EROD, Sigma-Aldrich) and 10 µM dicoumarol (Sigma-Aldrich) were added to the cells for 1 h. Subsequently, relative fluorescence of resorufin (excitation 535nm/emission 590nm) was measured either in form of an endpoint assay or as kinetic (kinetic reads every 30 min at 37°C, 5% CO₂) using an Infinite M200 pro reader platform (TECAN). EROD activity was corrected to the protein concentration measured by Bradford reaction (PierceTM Coomassie Plus Assay, Thermo Fisher Scientific) and normalized to the solvent control of the respective time point for end point assay. Endpoint assays are shown as Log₂ activity fold induction and kinetic measurements are shown as total well fluorescence over time.

LDH Release Assay. Release of lactate dehydrogenase (LDH) was quantified using the Cytotoxicity Detection Kit PLUS (Roche) according to the manufacturer's instructions. The percentage of cytotoxicity was calculated as:

$$\text{Cytotoxicity(\%)} = \frac{\text{experimental value} - \text{low control}}{\text{high control} - \text{low control}} \times 100$$

Caspase-3/7 Activity Assay. Caspase activity was measured using the CellEvent™ Caspase-3/7 Green Detection Reagent (Thermo Fisher Scientific) according to the manufacturer's instructions. In particular, after stimulation cell nuclei were labeled using NucRed™ Live 647 ReadyProbes™ Reagent (Thermo Fisher Scientific). Subsequently, cells were incubated with CellEvent™ Caspase-3/7 Green Detection Reagent for 30 min and micrographs were acquired using an ArrayScan™ XTI High Content Analysis Reader (Thermo Fisher Scientific). For subsequent analysis of Caspase-3/7 positive cells, nuclear labeling was used to identify and define cells and green fluorescence signal was used to determine caspase-3/7 positive cells.

***In vitro* Infections and Analysis.** For *in vitro* infections, *Mtb* H37Rv, *Mtb* H37Rv-GFP or *Mtb* patient isolates were cultured to an optical density at 600nm (OD_{600nm}) of 0.5-0.8 and single-cell suspensions prepared by collecting bacterial culture supernatants after centrifugation at 120 x g for 10 min. Bacterial CFU were calculated based on growth curves (OD_{600nm} of 1 equals approximately 2.5 x 10⁷ bacteria/ml). THP-1 macrophages were infected with cell culture medium containing a multiplicity of infection (MOI) of 10 for 4 h. After infection, bacteria not internalized were removed by rigorous washing with sterile DPBS (Gibco). For counting of CFU, cells were lysed using 0.1 % Triton X-100 (Sigma-Aldrich) in 1x DPBS (Gibco) and serial dilutions were prepared in 0.04 % Tween20 (Sigma-Aldrich) in 1x DPBS (Gibco). Bacterial dilutions were plated on Middlebrook 7H11 agar (BD) plates, sealed with parafilm®M (Merck) and incubated at 37°C for approximately 3 weeks. For the analysis of *Mtb*-GFP infected macrophages, cells were fixed using 4 % paraformaldehyde (PFA, Electron Microscopy Sciences) containing 1 µg/ml H33342 fluorescent DNA stain (Hoechst) in 1x DPBS (Gibco) for 30 min at 4°C and stored overnight in 2% PFA in 1x DPBS (Gibco) at 4°C. Micrographs were acquired using the ArrayScan™ XTI High

Content Analysis Reader (Thermo Fisher Scientific) and analysis was performed using the Cellomics® Compartmental Analysis V4 BioApplication (Thermo Fisher Scientific) of the HCS Studio software (SCR_016787, Thermo Fisher Scientific).

Broth Dilution Assay. To determine the minimal inhibitory concentration (MIC) of RFB in the presence or absence of CH-223191 in axenic mycobacterial cultures, we used the previously established broth dilution method (Wiegand, Hilpert and Hancock, 2008). *Mtb* H37Rv or *M. marinum*-Wasabi were cultured to an OD_{600nm} of 0.5-0.8 and subsequently diluted to an OD_{600nm} of 0.1 in their respective culture media. Cultures were diluted once more 1:50 in the respective culture medium and distributed to 96-well plates with round-bottom (Thermo Fisher Scientific). Bacteria were then incubated with different concentrations of RFB in the presence or absence of 12 µM CH-223191. After 7 d for *Mtb* H37Rv and after 4 d for *M. marinum* cultures, 10µl resazurin dye (AlamarBlue™; Thermo Fisher Scientific) was added to each well and incubated overnight. On the next day, supernatants were transferred to 96-well plates with clear flat-bottom and absorbance was measured at 570nm using a GloMax Microplate Reader (Promega). Correction wavelength was acquired at 600nm. MICs were determined by comparing the absorbance to culture negative background controls.

Zymosan-pHrodo Phagocytosis Assays. Zymosan is a protein-carbohydrate complex extracted from the cell wall of the yeast *S. cerevisiae*. We used zymosan conjugated to pHrodo (Thermo Fisher Scientific), a pH-sensitive fluorescent dye that increases its brightness in acidic environments. THP-1 macrophages were pre-stimulated with different compounds as depicted in figure legends. After stimulation, supernatants were removed and cells incubated with 0.5 mg/ml pHrodo Red zymosan A BioParticles conjugate (Thermo Fisher Scientific) in 1 x Live Cell Imaging Solution (Thermo Fisher Scientific) for 2 h. Cells were washed rigorously with

554 1x DPBS and fixed with 2 % PFA containing 1 µg/ml H33342 fluorescent DNA stain (Hoechst) in
555 1x DPBS (Gibco) for 30 min at 4°C, protected from exposure to light. Micrographs were acquired
556 using the ArrayScan™ XTI High Content Analysis Reader (Thermo Fisher Scientific) and analysis
557 was performed using the Cellomics® Compartmental Analysis V4 BioApplication (Thermo Fisher
558 Scientific) of the HCS Studio software (SCR_016787, Thermo Fisher Scientific). Results are
559 shown as mean of total pHrodo zymosan fluorescence intensity per cell of a 40 field acquisition
560 area acquired with a 20x objective.

561 **Rifabutin Metabolism.** Differentiated HepaRG cells or 2 dpf zebrafish embryos were stimulated
562 with 10µM RFB in the culture medium or zebrafish water, respectively. At different time points,
563 supernatants or fish water were collected and used for analysis by ultra-performance liquid
564 chromatography (UPLC). RFB was extracted by adding chloroform/methanol (2:1). After mixing
565 and centrifugation, the organic lower phase was collected and evaporated in a vacuum concentrator.
566 Dried samples were dissolved in 50% methanol, 0.1% formic acid. Subsequently, the RFB extracts
567 were loaded onto an HSSC18 reversed phase UPLC column. RFB was eluted with a linear gradient
568 of 15% acetonitrile to 90% acetonitrile (containing 0.1% formic acid) over 5 min at 45°C and a
569 flow rate of 0.6 ml/min. Eluted compounds were detected by UV absorbance and by ESI-MS
570 detection. RFB was detected by single ion recording (SIR) of m/z 847.5. The ESI-MS detection
571 was operated in an electrospray positive ion mode with a voltage of 0.8 kV, a cone voltage of 15 V
572 and a probe temperature of 600°C. A full mass spectrum between m/z 100 and m/z 1200 was
573 acquired at a sampling rate of 8.0 points/sec. Quantification of RFB was performed by integration
574 of the UV-absorbance peak at 360nm based on a seven point calibration from 1 pmol to 500 pmol
575 of RFB.

Molecular Modeling. First, the conformational space of RFB and RIF was analyzed with the conformational search tool of Maestro (SCR_016748, Version 11.8, Schroedinger), carried out with standard settings as mixed torsional / low-mode sampling. 122 different conformations were found for RFB and 155 for RIF. RFB, RIF and the AhR-inhibitor CH-223191 were docked into the previous described molecular monomer model of PasB-hAhR (Moura-Alves *et al.*, 2014), utilizing the induced fit docking method of Maestro (SCR_016748, Version 11.8, Schroedinger). Amine bonds of the ligands were allowed to vary in conformation and the ring conformations were sampled with an energy window of 6 kcal/mol. To allow for more room in the binding pocket, during the induced fit procedure several side chains covering the binding pocket of AhR (RFB: residues H291, F295, C300, M340, M348, F351; RIF: F287, T289, H291, F295, L308, Y322, Y322, I325, C333, M340, M348, F351, L353, V363, S365, I379, V381) were substituted with alanine (trimmed) in the initial docking step. In the second step these trimmed residues were reconstituted and refined together with amino acids located 5.0 Å around the initial ligand pose before the Glide re-docking (third step). The binding energy of the different molecules (ΔG binding) was calculated using the Prime MM-GBSA tool of Maestro (SCR_016748, Version 11.8, Schroedinger). Heterodimer models of hAhR and Arnt each comprising HLH / PasA / PasB domains were generated based on crystal structures on one hand of the homologous Hif2a / ARNT complex (Wu *et al.*, 2015) including dynamic studies thereof (Motta *et al.*, 2018) and on the other hand of the CLOCK/Bmal1 complex (Huang *et al.*, 2012). Structural images were generated with PyMOL Molecular Graphics System (SCR_000305, Version 1.8.4.1, Schroedinger)

AhR Binding Studies using MST. A codon-optimized fragment of human AhR encoding amino acid residues 23–475 was commercially synthesized (MWG Eurofins) and cloned into pET21b (Novagen) using NcoI and XhoI restriction sites. The pET30-EK/LIC-mArnt expression plasmid

599 encoding the murine Arnt (residues 85-465) was a kind gift from Oliver Daumke (MDC Berlin).
600 For protein expression, BL21(DE3) cells were co-transformed with both plasmids. Bacteria were
601 grown to OD_{600nm} of 0.6 in LB medium and protein expression was induced with 0.5 mM
602 isopropyl- β -D-thiogalactopyranoside (IPTG), followed by overnight expression at 18°C. Proteins
603 were purified as previously described (Huang *et al.*, 2012). Specifically, cell pellets were
604 resuspended in lysis buffer containing DNaseI (Serva) and Complete Protein Inhibitor Cocktail
605 (Roche) and lysed using a French Press. The clarified lysate was applied onto a HisTALON™
606 Superflow™ column (Clontech) and bound protein was eluted with increasing concentrations
607 of imidazole. Elution fractions were buffer exchanged and N-terminal 6xHis-tags were removed
608 with PreScission protease overnight at 4°C. Cleaved protein complex was further purified on a
609 HiTrap Heparin HP column (GE Healthcare), followed by SEC on a Superdex 200 10/300 GL
610 equilibrated in 20 mM HEPES pH 8.0, 200 mM NaCl, 5% glycerol, and 5 mM DTT. Peak fractions
611 containing AhR-Arnt were pooled and concentrated using Amicon filter units (Millipore).

612 Binding studies using purified AhR-Arnt complex were performed by microscale thermophoresis
613 (MST) using the Monolith® NT.LabelFree (NanoTemper Technologies GmbH). MST
614 measurements were performed according to the manufacturer's instructions. In particular, a
615 constant protein concentration of 250 nM diluted in assay buffer including 0.1% Pluronic F-127
616 was used. To this, a serial dilution of ligand dissolved in DMSO was added. After short incubation,
617 samples were filled into NT LabelFree Zero Background MST Premium coated capillaries
618 (NanoTemper Technologies GmbH). Measurements were carried out at 22°C. MST traces were
619 collected with an LED excitation power of 20% and a MST laser power of 20-40%. For analyzing
620 the interaction affinity, the dissociation constant (K_d) for each ligand was calculated using the

NanoTemper Analysis software by plotting changes in the normalized fluorescence (ΔF_{norm} [%]) as a function of the ligand concentration.

Zebrafish Chemical Stimulations. In stimulation experiments, 2 dpf embryos were treated with different compounds in E3 medium for the durations indicated in the respective figures. In experiments using the AhR inhibitor CH-223191 (Sigma-Aldrich), embryos were pre-exposed to 10 μM CH-223191 in E3 for 2 h prior to the experiment and the inhibitor was present during the entire duration of the experiment.

Zebrafish Cyp1a Enzymatic Activity. EROD experiments were conducted as previously described (Nacci *et al.*, 1998). In detail, during the assay non-fluorescent 7-ethoxyresorufin diffuses into the embryo where it is converted by Cyp1a to the fluorescent product resorufin. After compound stimulation or immersion with *M. marinum*, 2 dpf zebrafish embryos were washed and placed in E3 medium containing 0.4 $\mu\text{g/ml}$ of 7-ethoxyresorufin (Cayman Chemical) for 5 min. After incubation, embryos were anesthetized with 200 $\mu\text{g/ml}$ tricaine (MS-222, Sigma-Aldrich) and placed in black 96-well plates with clear bottom (Thermo Fisher Scientific) and micrographs were acquired using the ArrayScanTM XTI High Content Analysis Reader (Thermo Fisher Scientific). Brightfield images were used to identify embryo outlines and embryo fluorescence (filters excitation: 549/15nm, emission: 590-624nm) was determined as a readout of Cyp1a activation using the Cellomics® Zebratox BioApplication (Thermo Scientific) of the HCS Studio software (SCR_016787, Thermo Fisher Scientific).

Zebrafish Toxicity. For the assessment of compound toxicity for zebrafish embryos, brightfield images were acquired using the ArrayScanTM XTI High Content Analysis Reader (Thermo Fisher Scientific). To evaluate toxicity, the Cellomics® Zebratox BioApplication (Thermo Fisher

Scientific) of the HCS Studio software (SCR_016787, Thermo Fisher Scientific) was used. Head-to-tail distance and embryo straightness served as measure for compound toxicity.

Zebrafish Infection. In infection by immersion experiments, 2 dpf embryos were placed in E3 medium inoculated with different concentrations of *M. marinum* E11 and incubated at 28°C for time of the experiment. Inoculum preparations and infection by intravenous injection of zebrafish embryos were performed as described (Benard *et al.*, 2012). In particular, a colony of *M. marinum*-Wasabi was resuspended in 10 ml Middlebrook 7H9 broth (BD) containing 10% ADC (BD), 0.05% Tween 80 (Sigma-Aldrich) and 50 µg/ml hygromycin (Sigma-Aldrich). The culture was set to an OD_{600nm} of 0.2-0.3 and cultured statically overnight at 28°C. On the day of infection, OD was measured again to ensure the logarithmic growth phase of the culture and bacteria were harvested by centrifuging and washing 3 times in sterile 1x PBS. Based on previous growth curves, an OD_{600nm} of 1 corresponded to approximately 10⁸ *M. marinum*/ml and was used to determine CFU for infection. Bacteria were centrifuged and resuspended in 2% polyvinylpyrrolidone (PVP40, Sigma-Aldrich) in PBS (w/v) to the desired concentration. Before infection, zebrafish embryos were staged at 28 hpf based on morphological criteria. Anesthesia was induced using 200 µg/ml tricaine (MS-222, Sigma-Aldrich) approximately 10 min prior to infection. Borosilicate glass microcapillaries (Science Products GmbH BF100-78-10, with filament) were loaded with the bacterial inoculum using a microloader tip and subsequently mounted to a micromanipulator (Sutter Instrument, MM-33) with stand (World precision Instruments, M10L magnetic stand). Injections were performed using a FemtoJet microinjector (Eppendorf) under a Leica M50 stereomicroscope (Leica). Anesthetized embryos were positioned on a flat 1% agarose plate and a scale bar was used to determine the desired injection volume of approximately 1 nl/embryo.

200 CFU Wasabi-expressing *M. marinum* were injected into the caudal vein of a single embryo. After infection embryos were rested for 30 min in E3 medium at 28°C.

RFB Treatment of *M. marinum*-Infected Zebrafish. Infected zebrafish embryos were pooled and randomly distributed into different experimental groups. Embryos were incubated in either 10 µM CH-223191 or DMSO at 28°C for 2 h. Subsequently, embryos were treated once with either 5 µM or 10 µM RFB, or with DMSO as untreated control. Treatment was applied by adding RFB directly to the medium. At 4 d post infection (dpi), embryos were anesthetized and imaged using a stereomicroscope (MZ16FA, Leica) equipped with a DFC3000Gdigital color camera (Leica). Brightfield and fluorescence stereomicroscopy overlays were created using Adobe Photoshop (SCR_014199, Photoshop CS5, Adobe). To quantify the amount of fluorescent bacteria, bacterial pixel counts were determined and analyzed using Zebrafish Bacterial Load Analyzer software (Version 4, A. Nezhinsky, University Leiden Institute of Advanced Computer Science, Leiden, The Netherlands).

QUANTIFICATION AND STATISTICAL ANALYSIS

For *in vivo* experiments, zebrafish embryos were randomly assigned to different experimental groups and group size was chosen to allow a significance threshold α of 0.05 with a power of 80% ($\beta= 0.2$). For *in vitro* experiments, cells were randomly distributed in different culture well plate positions. All statistical details of experiments can be found in the figure legends. Data are presented as mean \pm SD (for individual experiments) or as mean \pm SEM (for pooled experiments), as described in figure legends. To compute P values, unpaired t test or Mann-Whitney test was

686 used, as described in figure legends. GraphPad Prism (SCR_002798, version 7.0, GraphPad) was
687 used for analysis and differences were considered statistically significant at $P \leq 0.05$.

688 **DATA AND CODE AVAILABILITY**

689 This study did not generate any unique datasets or code.

690

691

692 **References**

- 693 Alcaide, J., Altet, M. N., Plans, P., Parrón, I., Folguera, L., Saltó, E., Domínguez, A., Pardell, H.
694 and Salleras, L. (1996) “Cigarette smoking as a risk factor for tuberculosis in young adults: a case-
695 control study.,” *Tubercle and lung disease : the official journal of the International Union against*
696 *Tuberculosis and Lung Disease*, 77(2), pp. 112–6. doi: 10.1016/s0962-8479(96)90024-6.
- 697 Angeles-Floriano, T., Roa-Espitia, A. L., Baltiérrez-Hoyos, R., Cordero-Martínez, J., Elizondo, G.
698 and Hernández-González, E. O. (2016) “Absence of aryl hydrocarbon receptor alters CDC42
699 expression and prevents actin polymerization during capacitation.,” *Molecular reproduction and*
700 *development*, 83(11), pp. 1015–1026. doi: 10.1002/mrd.22736.
- 701 Baquero, F., Negri, M. C., Morosini, M. I. and Blázquez, J. (1997) “The antibiotic selective
702 process: concentration-specific amplification of low-level resistant populations.,” *Ciba Foundation*
703 *symposium*, 207, pp. 93-105–11. doi: 10.1002/9780470515358.ch7.
- 704 Benard, E. L., van der Sar, A. M., Ellett, F., Lieschke, G. J., Spaink, H. P. and Meijer, A. H. (2012)
705 “Infection of zebrafish embryos with intracellular bacterial pathogens.,” *Journal of visualized*
706 *experiments : JoVE*. MyJoVE Corporation, (61). doi: 10.3791/3781.
- 707 Bode, C., Diedrich, B., Muenster, S., Hentschel, V., Weisheit, C., Rommelsheim, K., Hoeft, A.,
708 Meyer, R., Boehm, O., Knuefermann, P. and Baumgarten, G. (2014) “Antibiotics regulate the
709 immune response in both presence and absence of lipopolysaccharide through modulation of Toll-
710 like receptors, cytokine production and phagocytosis in vitro,” *International*
711 *Immunopharmacology*, 18, pp. 27–34. doi: 10.1016/j.intimp.2013.10.025.
- 712 Carvajal-Gonzalez, J. M., Mulero-Navarro, S., Roman, A. C., Sauzeau, V., Merino, J. M., Bustelo,
713 X. R. and Fernandez-Salguero, P. M. (2009) “The dioxin receptor regulates the constitutive
714 expression of the vav3 proto-oncogene and modulates cell shape and adhesion.,” *Molecular biology*
715 *of the cell*, 20(6), pp. 1715–27. doi: 10.1091/mbc.e08-05-0451.
- 716 Cervantes-Barragan, L., Chai, J. N., Tianero, M. D., Di Luccia, B., Ahern, P. P., Merriman, J.,
717 Cortez, V. S., Caparon, M. G., Donia, M. S., Gilfillan, S., Cella, M., Gordon, J. I., Hsieh, C.-S. and
718 Colonna, M. (2017) “*Lactobacillus reuteri* induces gut intraepithelial CD4⁺ CD8αα⁺ T cells,”
719 *Science*, 357(6353), pp. 806–810. doi: 10.1126/science.aah5825.
- 720 Corrada, D., Denison, M. S. and Bonati, L. (2017) “Structural modeling of the AhR:ARNT
721 complex in the bHLH–PASA–PASB region elucidates the key determinants of dimerization,”
722 *Molecular BioSystems*. The Royal Society of Chemistry, 13(5), pp. 981–990. doi:
723 10.1039/C7MB00005G.
- 724 Corrada, D., Soshilov, A. A., Denison, M. S. and Bonati, L. (2016) “Deciphering Dimerization
725 Modes of PAS Domains: Computational and Experimental Analyses of the AhR:ARNT Complex
726 Reveal New Insights Into the Mechanisms of AhR Transformation,” *PLOS Computational Biology*.
727 Edited by O. Keskin. Public Library of Science, 12(6), p. e1004981. doi:
728 10.1371/journal.pcbi.1004981.
- 729 Dalton, J. P., Uy, B., Okuda, K. S., Hall, C. J., Denny, W. A., Crosier, P. S., Swift, S. and Wiles,
730 S. (2017) “Screening of anti-mycobacterial compounds in a naturally infected zebrafish larvae

731 model,” *Journal of Antimicrobial Chemotherapy*. Oxford University Press, 72(2), pp. 421–427.
732 doi: 10.1093/jac/dkw421.

733 DeRyke, C. A., Young Lee, S., Kuti, J. L. and Nicolau, D. P. (2006) “Optimising Dosing Strategies
734 of Antibacterials Utilising Pharmacodynamic Principles,” *Drugs*, 66(1), pp. 1–14. doi:
735 10.2165/00003495-200666010-00001.

736 Evans, B. R., Karchner, S. I., Franks, D. G. and Hahn, M. E. (2005) “Duplicate aryl hydrocarbon
737 receptor repressor genes (ahrr1 and ahrr2) in the zebrafish *Danio rerio*: Structure, function,
738 evolution, and AHR-dependent regulation in vivo,” *Archives of Biochemistry and Biophysics*,
739 441(2), pp. 151–167. doi: 10.1016/j.abb.2005.07.008.

740 Gengenbacher, M. and Kaufmann, S. H. E. (2012) “*Mycobacterium tuberculosis* : success through
741 dormancy,” *FEMS Microbiology Reviews*. Wiley/Blackwell (10.1111), 36(3), pp. 514–532. doi:
742 10.1111/j.1574-6976.2012.00331.x.

743 Guillouzo, A., Corlu, A., Aninat, C., Glaise, D., Morel, F. and Guguen-Guillouzo, C. (2007) “The
744 human hepatoma HepaRG cells: A highly differentiated model for studies of liver metabolism and
745 toxicity of xenobiotics,” *Chemico-Biological Interactions*. Elsevier, 168(1), pp. 66–73. doi:
746 10.1016/J.CBI.2006.12.003.

747 Gutiérrez-Vázquez, C. and Quintana, F. J. (2018) “Regulation of the Immune Response by the Aryl
748 Hydrocarbon Receptor,” *Immunity*. NIH Public Access, 48(1), pp. 19–33. doi:
749 10.1016/j.immuni.2017.12.012.

750 Huang, N., Chelliah, Y., Shan, Y., Taylor, C. A., Yoo, S.-H., Partch, C., Green, C. B., Zhang, H.
751 and Takahashi, J. S. (2012) “Crystal Structure of the Heterodimeric CLOCK:BMAL1
752 Transcriptional Activator Complex,” *Science*, 337(6091), pp. 189–194. doi:
753 10.1126/science.1222804.

754 Hubbard, T. D., Murray, I. A. and Perdew, G. H. (2015) “Special Section on Drug Metabolism and
755 the Microbiome—Minireview Indole and Tryptophan Metabolism: Endogenous and Dietary
756 Routes to Ah Receptor Activation,” *DRUG METABOLISM AND DISPOSITION Drug Metab*
757 *Dispos*, 43, pp. 1522–1535. doi: 10.1124/dmd.115.064246.

758 Kaufmann, S. H. E., Dorhoi, A., Hotchkiss, R. S. and Bartenschlager, R. (2018) “Host-directed
759 therapies for bacterial and viral infections,” *Nature Reviews Drug Discovery*. Nature Publishing
760 Group, 17(1), pp. 35–56. doi: 10.1038/nrd.2017.162.

761 Kaufmann, S. H., Rubin, E. and Zumla, A. (2015) *Tuberculosis*. Cold Spring Harbor: Cold Spring
762 Harbor Laboratory Press.

763 Kawajiri, K. and Fujii-Kuriyama, Y. (2016) “The aryl hydrocarbon receptor: a multifunctional
764 chemical sensor for host defense and homeostatic maintenance,” *Experimental Animals*, (66 (2)),
765 pp. 75–89. doi: 10.1538/expanim.16-0092.

766 Kim, S.-H., Henry, E. C., Kim, D.-K., Kim, Y.-H., Shin, K. J., Han, M. S., Lee, T. G., Kang, J.-K.,
767 Gasiewicz, T. A., Ryu, S. H. and Suh, P.-G. (2006) “Novel Compound 2-Methyl-2H-pyrazole-3-
768 carboxylic Acid (2-methyl-4-o-tolylazo-phenyl)-amide (CH-223191) Prevents 2,3,7,8-TCDD-
769 Induced Toxicity by Antagonizing the Aryl Hydrocarbon Receptor,” *Molecular Pharmacology*,

69(6), pp. 1871–1878. doi: 10.1124/mol.105.021832.

Kolloli, A. and Subbian, S. (2017) “Host-Directed Therapeutic Strategies for Tuberculosis,” *Frontiers in medicine*. Frontiers Media SA, 4, p. 171. doi: 10.3389/fmed.2017.00171.

Van Leeuwen, L. M., Van Der Sar, A. M. and Bitter, W. (2015) *Animal Models of Tuberculosis: Zebrafish*. doi: 10.1101/cshperspect.a018580.

Leung, C. C., Yew, W. W., Chan, C. K., Chang, K. C., Law, W. S., Lee, S. N., Tai, L. B., Leung, E. C. C., Au, R. K. F., Huang, S. S. and Tam, C. M. (2015) “Smoking adversely affects treatment response, outcome and relapse in tuberculosis,” *The European respiratory journal*. European Respiratory Society, 45(3), pp. 738–45. doi: 10.1183/09031936.00114214.

Liew, W. C. and Orban, L. (2014) “Zebrafish sex: a complicated affair,” *Briefings in Functional Genomics*, 13(2), pp. 172–187. doi: 10.1093/bfpg/elt041.

Lozza, L., Moura-Alves, P., Domaszewska, T., Lage Crespo, C., Streat, I., Kreuchwig, A., Puyskens, A., Bechtle, M., Klemm, M., Zedler, U., Silviu Ungureanu, B., Gühlich-Bornhof, U., Koehler, A.-B., Stäber, M., Mollenkopf, H.-J., Hurwitz, R., Furkert, J., Krause, G., Weiner, J., Jacinto, A., Mihai, I., Leite-de-Moraes, M., Siebenhaar, F., Maurer, M. and Kaufmann, S. H. E. (2019) “The Henna pigment Lawsone activates the Aryl Hydrocarbon Receptor and impacts skin homeostasis,” *Scientific Reports*. Nature Publishing Group, 9(1), p. 10878. doi: 10.1038/s41598-019-47350-x.

Mahiout, S., Tagliabue, S. G., Nasri, A., Omoruyi, I. M., Pettersson, L., Bonati, L. and Pohjanvirta, R. (2018) “In vitro toxicity and in silico docking analysis of two novel selective AH-receptor modulators,” *Toxicology in Vitro*. Elsevier Ltd, 52, pp. 178–188. doi: 10.1016/j.tiv.2018.06.010.

Martey, C. A., Baglole, C. J., Gasiewicz, T. A., Sime, P. J. and Phipps, R. P. (2005) “The aryl hydrocarbon receptor is a regulator of cigarette smoke induction of the cyclooxygenase and prostaglandin pathways in human lung fibroblasts,” *American Journal of Physiology-Lung Cellular and Molecular Physiology*. American Physiological Society, 289(3), pp. L391–L399. doi: 10.1152/ajplung.00062.2005.

Mitchison, D. A. (1998) “How drug resistance emerges as a result of poor compliance during short course chemotherapy for tuberculosis,” *The international journal of tuberculosis and lung disease: the official journal of the International Union against Tuberculosis and Lung Disease*, 2(1), pp. 10–5.

Mohammadi-Bardbori, A. and Mohammadi-Bardbori, A. (2014) “Assay for quantitative determination of CYP1A1 enzyme activity using 7-Ethoxyresorufin as standard substrate (EROD assay),” *Protocol Exchange*. doi: 10.1038/protex.2014.043.

Motta, S., Minici, C., Corrada, D., Bonati, L. and Pandini, A. (2018) “Ligand-induced perturbation of the HIF-2 α :ARNT dimer dynamics,” *PLOS Computational Biology*. Edited by O. Keskin. Public Library of Science, 14(2), p. e1006021. doi: 10.1371/journal.pcbi.1006021.

Moura-Alves, P., Faé, K., Houthuys, E., Dorhoi, A., Kreuchwig, A., Furkert, J., Barison, N., Diehl, A., Munder, A., Constant, P., Skrahina, T., Gühlich-Bornhof, U., Klemm, M., Koehler, A.-B., Bandermann, S., Goosmann, C., Mollenkopf, H.-J., Hurwitz, R., Brinkmann, V., Fillatreau, S.,

809 Daffe, M., Tümmler, B., Kolbe, M., Oschkinat, H., Krause, G. and Kaufmann, S. H. E. (2014)
810 "AhR sensing of bacterial pigments regulates antibacterial defence," *Nature*, 512. doi:
811 10.1038/nature13684.

812 Muto, H. and Takizawa, Y. (1989) "Dioxins in Cigarette Smoke," *Archives of Environmental*
813 *Health: An International Journal*, 44(3), pp. 171–174. doi: 10.1080/00039896.1989.9935882.

814 Nacci, D., Coiro, L., Kuhn, A., Champlin, D., Munns, W., Specker, J. and Cooper, K. (1998)
815 "Nondestructive indicator of ethoxyresorufin- *O* -deethylase activity in embryonic fish,"
816 *Environmental Toxicology and Chemistry*. Wiley-Blackwell, 17(12), pp. 2481–2486. doi:
817 10.1002/etc.5620171214.

818 Nebert, D. W., Goujon, F. M. and Gielen, J. E. (1972) "Aryl hydrocarbon hydroxylase induction
819 by polycyclic hydrocarbons: simple autosomal dominant trait in the mouse.," *Nature: New biology*,
820 236(65), pp. 107–10.

821 Negri, M. C., Lipsitch, M., Blázquez, J., Levin, B. R. and Baquero, F. (2000) "Concentration-
822 dependent selection of small phenotypic differences in TEM beta-lactamase-mediated antibiotic
823 resistance.," *Antimicrobial agents and chemotherapy*, 44(9), pp. 2485–91.

824 Nishida, M., Mine, Y., Nonoyama, S. and Yokota, Y. (1976) "Effect of antibiotics on the
825 phagocytosis and killing of *Pseudomonas aeruginosa* by rabbit polymorphonuclear leukocytes.,"
826 *Chemotherapy*. Karger Publishers, 22(3–4), pp. 203–10. doi: 10.1159/000221927.

827 Nüsslein-Volhard, C. and Dahm, R. (2002) *Zebrafish : a practical approach*. Oxford University
828 Press.

829 Olofsson, S. K. and Cars, O. (2007) "Optimizing Drug Exposure to Minimize Selection of
830 Antibiotic Resistance," *Clinical Infectious Diseases*. Oxford University Press, 45(Supplement_2),
831 pp. S129–S136. doi: 10.1086/519256.

832 Parks, A. J., Pollastri, M. P., Hahn, M. E., Stanford, E. A., Novikov, O., Franks, D. G., Haigh, S.
833 E., Narasimhan, S., Ashton, T. D., Hopper, T. G., Kozakov, D., Beglov, D., Vajda, S., Schlezinger,
834 J. J. and Sherr, D. H. (2014) "In Silico Identification of an Aryl Hydrocarbon Receptor Antagonist
835 with Biological Activity In Vitro and In Vivo," *Molecular Pharmacology*, 86(5), pp. 593–608. doi:
836 10.1124/mol.114.093369.

837 Pfaffl, M. W. (2001) *A new mathematical model for relative quantification in real-time RT-PCR*,
838 *Nucleic Acids Research*. doi: 10.1093/nar/29.9.e45.

839 Pohjanvirta, R. (2011) *The AH receptor in biology and toxicology*. Edited by R. Pohjanvirta. Wiley.
840 doi: 10.1002/9781118140574.

841 Poland, A., Glover, E. and Kende, A. S. (1976) "Stereospecific, high affinity binding of 2,3,7,8-
842 tetrachlorodibenzo-*p*-dioxin by hepatic cytosol. Evidence that the binding species is receptor for
843 induction of aryl hydrocarbon hydroxylase.," *The Journal of biological chemistry*, 251(16), pp.
844 4936–46.

845 Poland, A. and Knutson, J. C. (1982) "2,3,7,8-Tetrachlorodibenzo- *p* -Dioxin and Related
846 Halogenated Aromatic Hydrocarbons: Examination of the Mechanism of Toxicity," *Annual Review*

847 of *Pharmacology and Toxicology*, 22(1), pp. 517–554. doi:
848 10.1146/annurev.pa.22.040182.002505.

849 Prasch, A. L., Teraoka, H., Carney, S. A., Dong, W., Hiraga, T., Stegeman, J. J., Heideman, W.
850 and Peterson, R. E. (2003) “Aryl Hydrocarbon Receptor 2 Mediates 2,3,7,8-Tetrachlorodibenzo-
851 p-dioxin Developmental Toxicity in Zebrafish,” *Toxicological Sciences*. Oxford University Press,
852 76(1), pp. 138–150. doi: 10.1093/toxsci/kfg202.

853 Queval, C. J., Song, O.-R., Carralot, J.-P., Saliou, J.-M., Bongiovanni, A., Deloison, G., Deboosère,
854 N., Jouny, S., Iantomasi, R., Delorme, V., Debrie, A.-S., Park, S.-J., Gouveia, J. C., Tomavo, S.,
855 Brosch, R., Yoshimura, A., Yeramian, E. and Brodin, P. (2017) “Mycobacterium tuberculosis
856 Controls Phagosomal Acidification by Targeting CISH-Mediated Signaling,” *Cell Reports*. Cell
857 Press, 20(13), pp. 3188–3198. doi: 10.1016/J.CELREP.2017.08.101.

858 Rangel Moreno, J., Estrada García, I., De La Luz García Hernández, M., Aguilar Leon, D.,
859 Marquez, R. and Hernández Pando, R. (2002) “The role of prostaglandin E2 in the
860 immunopathogenesis of experimental pulmonary tuberculosis,” *Immunology*, 106(2), pp. 257–66.
861 doi: 10.1046/j.1365-2567.2002.01403.x.

862 Roper, C. and Tanguay, R. L. (2018) “Zebrafish as a Model for Developmental Biology and
863 Toxicology,” *Handbook of Developmental Neurotoxicology*. Academic Press, pp. 143–151. doi:
864 10.1016/B978-0-12-809405-1.00012-2.

865 Rowland, M. and Tozer, T. N. (2011) *Clinical Pharmacokinetics and Pharmacodynamics*
866 *Concepts and Applications*. Fourth Edi, *Pharmaceutical Sciences*. Fourth Edi. Wolters Kluwer
867 Health/Lippincott William & Wilkins. doi: 10.1111/j.1469-0691.2010.03358.x.

868 Seidel, S. A. I., Dijkman, P. M., Lea, W. A., van den Bogaart, G., Jerabek-Willemsen, M., Lazic,
869 A., Joseph, J. S., Srinivasan, P., Baaske, P., Simeonov, A., Katritch, I., Melo, F. A., Ladbury, J. E.,
870 Schreiber, G., Watts, A., Braun, D. and Duhr, S. (2013) “Microscale thermophoresis quantifies
871 biomolecular interactions under previously challenging conditions,” *Methods*, 59(3), pp. 301–315.
872 doi: 10.1016/j.ymeth.2012.12.005.

873 Smith, S. H., Jayawickreme, C., Rickard, D. J., Nicodeme, E., Bui, T., Simmons, C., Coquery, C.
874 M., Neil, J., Pryor, W. M., Mayhew, D., Rajpal, D. K., Creech, K., Furst, S., Lee, J., Wu, D.,
875 Rastinejad, F., Willson, T. M., Viviani, F., Morris, D. C., Moore, J. T. and Cote-Sierra, J. (2017)
876 “Tapinarof Is a Natural AhR Agonist that Resolves Skin Inflammation in Mice and Humans,”
877 *Journal of Investigative Dermatology*, 137(10), pp. 2110–2119. doi: 10.1016/j.jid.2017.05.004.

878 Solis, N. V., Swidergall, M., Bruno, V. M., Gaffen, S. L. and Filler, S. G. (2017) “The Aryl
879 Hydrocarbon Receptor Governs Epithelial Cell Invasion during Oropharyngeal Candidiasis,”
880 *mBio*. American Society for Microbiology (ASM), 8(2). doi: 10.1128/mBio.00025-17.

881 Stedman, R. L. (1968) “Chemical composition of tobacco and tobacco smoke,” *Chemical Reviews*.
882 American Chemical Society, 68(2), pp. 153–207. doi: 10.1021/cr60252a002.

883 Stockinger, B., Meglio, P. Di, Gialitakis, M. and Duarte, J. H. (2014) “The Aryl Hydrocarbon
884 Receptor: Multitasking in the Immune System,” *Annual Review of Immunology*. Annual Reviews
885 , 32(1), pp. 403–432. doi: 10.1146/annurev-immunol-032713-120245.

886 Takaki, K., Davis, J. M., Winglee, K. and Ramakrishnan, L. (2013) "Evaluation of the pathogenesis
887 and treatment of Mycobacterium marinum infection in zebrafish," *Nature Protocols*, 8(6), pp.
888 1114–1124. doi: 10.1038/nprot.2013.068.

889 Uchida, D., Yamashita, M., Kitano, T. and Iguchi, T. (2002) "Oocyte apoptosis during the
890 transition from ovary-like tissue to testes during sex differentiation of juvenile zebrafish," *The*
891 *Journal of experimental biology*, 205(Pt 6), pp. 711–8.

892 Wiegand, I., Hilpert, K. and Hancock, R. E. W. (2008) "Agar and broth dilution methods to
893 determine the minimal inhibitory concentration (MIC) of antimicrobial substances," *Nature*
894 *Protocols*. Nature Publishing Group, 3(2), pp. 163–175. doi: 10.1038/nprot.2007.521.

895 Wincent, E., Bengtsson, J., Bardbori, A. M., Alsberg, T., Luecke, S., Rannug, U. and Rannug, A.
896 (2012) "Inhibition of cytochrome P4501-dependent clearance of the endogenous agonist FICZ as
897 a mechanism for activation of the aryl hydrocarbon receptor," *Proceedings of the National*
898 *Academy of Sciences*, 109(12), pp. 4479–4484. doi: 10.1073/pnas.1118467109.

899 World Health Organization (2016) *WHO treatment guidelines for drug-resistant tuberculosis :*
900 *2016 update*. Geneva. doi: WHO/HTM/TB/2016.04.

901 World Health Organization (2019) *Global tuberculosis report 2019*. Geneva.

902 World Health Organization 2017 (2017) *Guidelines for treatment of drug-susceptible tuberculosis*
903 *and patient care, 2017 update*. Geneva.

904 Wu, D., Potluri, N., Lu, J., Kim, Y. and Rastinejad, F. (2015) "Structural integration in hypoxia-
905 inducible factors," *Nature*, 524(7565), pp. 303–308. doi: 10.1038/nature14883.

906 Yen, Y.-F., Yen, M.-Y., Lin, Y.-S., Lin, Y.-P., Shih, H.-C., Li, L.-H., Chou, P. and Deng, C.-Y.
907 (2014) "Smoking increases risk of recurrence after successful anti-tuberculosis treatment: a
908 population-based study," *The International Journal of Tuberculosis and Lung Disease*, 18(4), pp.
909 492–498. doi: 10.5588/ijtld.13.0694.

910 Yeste, A., Nadeau, M., Burns, E. J., Weiner, H. L. and Quintana, F. J. (2012) "Nanoparticle-
911 mediated codelivery of myelin antigen and a tolerogenic small molecule suppresses experimental
912 autoimmune encephalomyelitis," *Proceedings of the National Academy of Sciences*, 109(28), pp.
913 11270–11275. doi: 10.1073/pnas.1120611109.

914 Yeste, A., Takenaka, M. C., Mascanfroni, I. D., Nadeau, M., Kenison, J. E., Patel, B., Tukpah, A.-
915 M., Babon, J. A. B., DeNicola, M., Kent, S. C., Pozo, D. and Quintana, F. J. (2016) "Tolerogenic
916 nanoparticles inhibit T cell-mediated autoimmunity through SOCS2," *Science Signaling*, 9(433),
917 p. ra61-ra61. doi: 10.1126/scisignal.aad0612.

918 Zelante, T., Iannitti, R. G., Cunha, C., De Luca, A., Giovannini, G., Pieraccini, G., Zecchi, R.,
919 D'Angelo, C., Massi-Benedetti, C., Fallarino, F., Carvalho, A., Puccetti, P. and Romani, L. (2013)
920 "Tryptophan Catabolites from Microbiota Engage Aryl Hydrocarbon Receptor and Balance
921 Mucosal Reactivity via Interleukin-22," *Immunity*, 39(2), pp. 372–385. doi:
922 10.1016/j.immuni.2013.08.003.

923 Zhong, H. and Lin, S. (2011) "Chemical Screening with Zebrafish Embryos," in *Methods in*

924 *molecular biology* (Clifton, N.J.), pp. 193–205. doi: 10.1007/978-1-61779-012-6_12.

925

KEY RESOURCES TABLE

REAGENT or RESOURCE	SOURCE	IDENTIFIER
Bacterial and Virus Strains		
BL1(DE3) Competent <i>Escherichia coli</i>	New England Biolabs	Cat#C25271
<i>Mycobacterium tuberculosis</i> strain H37Rv	ATCC®	ATCC® 27294
<i>Mycobacterium tuberculosis</i> strain H37Rv-GFP	Lab collection; <i>Mtb</i> H37Rv strain expressing GFP with kanamycin resistance marker	N/A
<i>Mycobacterium tuberculosis</i> RIF-monoresistant patient isolate	Forschungszentrum Borstel	NRZ (FZB-DIAM):18000790
<i>Mycobacterium tuberculosis</i> drug-sensitive patient isolate	Forschungszentrum Borstel	NRZ (FZB-DIAM):18000880
<i>Mycobacterium marinum</i> strain E11	Lab collection; Puttinaowarat et al., 1999	N/A
<i>Mycobacterium marinum</i> strain M	ATCC®	ATCC® BAA-535™
<i>Mycobacterium marinum</i> strain M-Wasabi	Lab collection; Takaki et al., 2013	N/A
Chemicals, Peptides, and Recombinant Proteins		
2,3,7,8-Tetrachlorodibenzo- <i>p</i> -dioxin (TCDD)	LGC Standards	Cat#CIL-ED-901-C; CAS#1746-01-6
2-Hydroxy-3-methyl-1,4-naphthoquinone (Pht)	Sigma-Aldrich	Cat#S970840
2-Mercaptoethanol	Sigma-Aldrich	Cat#M6250; CAS#60-24-2
2-Methyl-N-[2-methyl-4-[(2-methylphenyl)diazeryl]phenyl]pyrazole-3-carboxamide (CH-223191)	Sigma-Aldrich	Cat#C8124; CAS#301326-22-7
3-Aminobenzoic acid (Tricaine; MS-222)	Sigma-Aldrich	Cat#127671; CAS#99-05-8
4-Aminosalicylic acid	Sigma-Aldrich	Cat#A79604; CAS#65-49-6
25-O-Deacetyl rifabutin (LM565)	Toronto Research Chemicals	Cat#D198980; CAS#100324-63-8
AlamarBlue™	Thermo Fisher Scientific	Cat#DAL1025
Amikacin	Sigma-Aldrich	Cat#1019508; CAS#37517-28-5
Bedaquiline (TMC-207)	AdooQ Bioscience LLC	Cat#A12327-5; CAS#843663-66-1
CellEvent™ Caspase-3/7 Green Detection Reagent	Thermo Fisher Scientific	Cat#C10423
Clofazimine	Sigma-Aldrich	Cat#C8895; CAS#2030-63-9
Complete™ Protein Inhibitor Cocktail	Roche	Cat#CO-RO
Dicoumarol	Sigma-Aldrich	Cat#287897; CAS#66-76-2
Enrofloxacin	Sigma-Aldrich	Cat#17849; CAS#93106-60-6
Ethambutol	Sigma-Aldrich	Cat#E4630; CAS#1070-11-7

Ethionamide	Sigma-Aldrich	Cat#E6005; CAS#536-33-4
Ethoxyresorufin	Sigma-Aldrich	Cat#E3763; CAS#5725-91-7
Hoechst 33342	Thermo Fisher Scientific	Cat#62249
Hygromycin	Sigma-Aldrich	Cat#H3274;CAS#31 282-04-9
Isoniazid	Sigma-Aldrich	Cat#I3377; CAS#54- 85-3
Kanamycin	Sigma-Aldrich	Cat#60615; CAS#70560-51-9
Linezolid	Sigma-Aldrich	Cat#PZ0014; CAS#165800-03-3
Live Cell Imaging Solution	Thermo Fisher Scientific	Cat#A14291DJ
Moxifloxacin	Sigma-Aldrich	Cat#32477; CAS#186826-86-8
NucRed™ Live 647 ReadyProbes™ Reagent	Thermo Fisher Scientific	Cat#R37106
Polyvinylpyrrolidone, avg. mol wt. 40,000 (PVP40)	Sigma-Aldrich	Cat#PVP40 CAS#9003-39-8
Phorbol 12-myristate 13-acetate (PMA)	Sigma-Aldrich	Cat#524400; CAS#16561-29-8
pHrodo™ Red Zymosan Bioparticles™ Conjugate	Thermo Fisher Scientific	Cat#P35364
Pronase	Sigma-Aldrich	Cat#PRON-RO
Puromycin	Sigma-Aldrich	Cat#P9620; CAS# 58-58-2
Pyrazinamide	Sigma-Aldrich	Cat#P4050000; CAS#98-96-4
Reporter Lysis Buffer	Promega	Cat#E4030
Rifabutin	Carbosynth	Cat#AR27727; CAS#72559-06-9
Rifampicin	Sigma-Aldrich	Cat#R3501; CAS#13292-46-1
Rifapentine	Sigma-Aldrich	Cat#R0533; CAS#61379-65-5
Streptomycin	Sigma-Aldrich	Cat#S6501; CAS#3810-74-0
SYBR green	Thermo Fisher Scientific	Cat#A25743
Thiacetazone	Santa Cruz Biotechnology	Cat#sc-358574; CAS#104-06-3
Critical Commercial Assays		
Cytotoxicity Detection Kit (LDH)	Roche	Cat#11644793001
iScript™ cDNA Synthesis Kit	Bio-Rad	Cat#1708891
Luciferase Assay System	Promega	Cat#E1501
Pierce™ Coomassie Plus (Bradford) Assay Kit	Thermo Fisher Scientific	Cat#23236
RNeasy® Mini Kit	Qiagen	Cat#74106
Experimental Models: Cell Lines		
Hepa-1c1c7	ATCC	RRID: CVCL_0328; CRL-2026

THP-1	ATCC	RRID: CVCL_0006; TIB-202
THP-1 AhR reporter	Moura-Alves et al., 2014	N/A
THP-1 AhR knockdown	Moura-Alves et al., 2014	N/A
HepaRG	Biopredic International	HPR101
Experimental Models: Organisms/Strains		
Zebrafish (<i>Danio rerio</i>) strain AB (wild-type line)	EZRC	ZFIN ID: ZDB-GENO-960809-7
Oligonucleotides		
codon-optimized fragment of human AhR encoding amino acid residues 23–475	This study	N/A
ON-TARGET plus Human AHR (NM_001621) siRNA	Dharmacon	Code L-004990-00-0005
ON-TARGET plus Non-targeting Pool siRNA	Dharmacon	Code D-001810-10-05
Primers used for qRT-PCR, see Table S3	This study	N/A
Recombinant DNA		
pET21b	Novagen	Cat#69741
pET30-EK/LIC-mARNT expression plasmid encoding the murine ARNT	A kind gift from Oliver Daumke, MDC Berlin	N/A
Software and Algorithms		
GraphPad Prism, Version 7.0	GraphPad	RRID: SCR_002798; https://www.graphpad.com/
HCS Studio Cell Analysis Software, Version 6.5.0	Thermo Fisher Scientific	RRID:SCR_016787; https://www.thermofisher.com/de/de/home/life-science/cell-analysis/cellular-imaging/high-content-screening/high-content-screening-instruments/hcs-studio-2.html
LightCycler® 480 Software	Roche	RRID:SCR_012155; https://lifescience.roche.com/en_de/products/lightcycler14301-480-software-version-15.html
i-control™	Tecan	N/A; https://lifesciences.tecan.com/plate_readers/infinite_200_pro?p=tab--3#
Maestro Suite, Version 11.8	Schrödinger	RRID:SCR_016748; https://www.schrodinger.com/maestro

NanoTemper Analysis software	NanoTemper Technologies	N/A; https://nanotemperte.ch.com/monolith-mo-control-software/
Photoshop CS5	Adobe	RRID:SCR_014199; https://www.adobe.com
PyMOL Molecular Graphics System, Version 1.8.4.1	Schrödinger	RRID:SCR_000305; https://pymol.org
Zebrafish Bacterial Load Analyzer software, Version 4	Nezhinsky et al., 2012	N/A

Figure 1

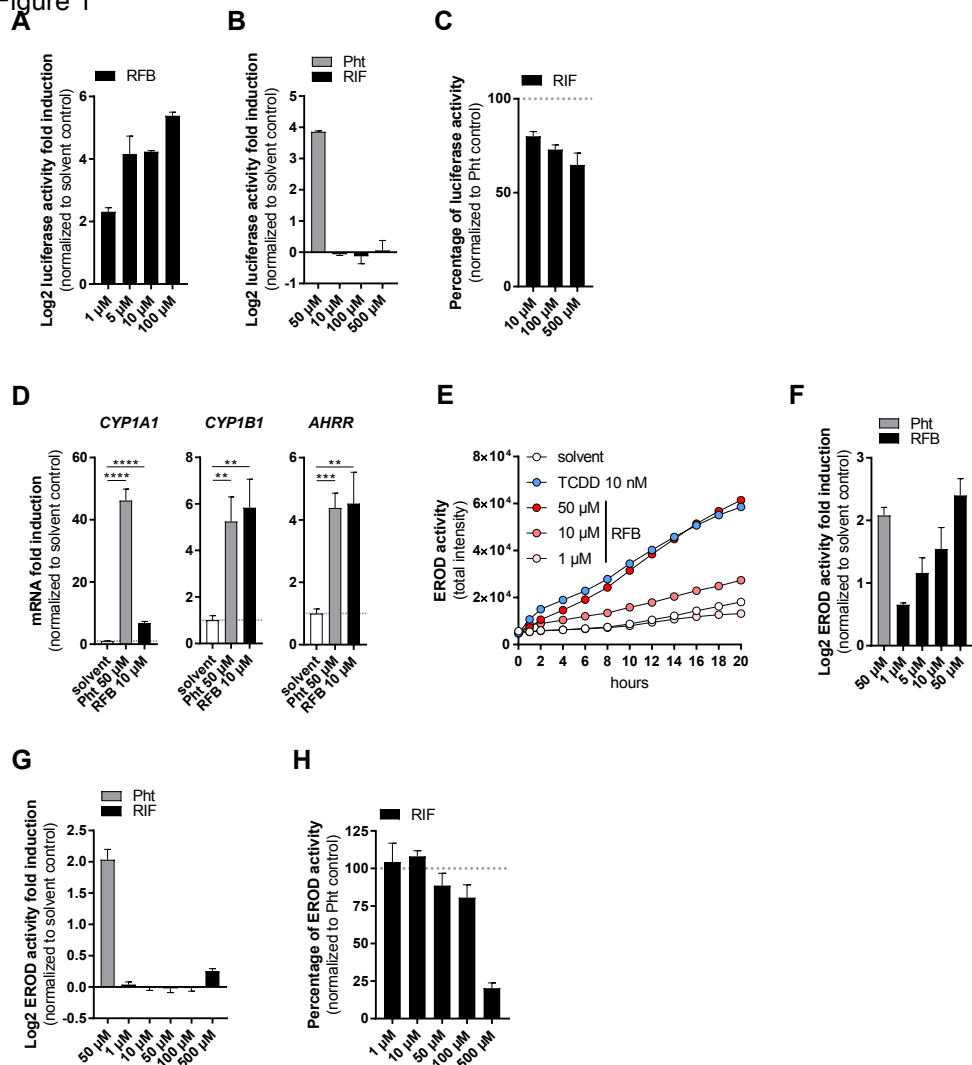
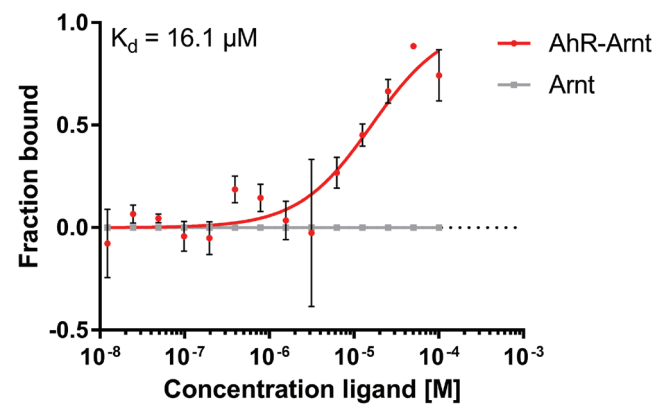


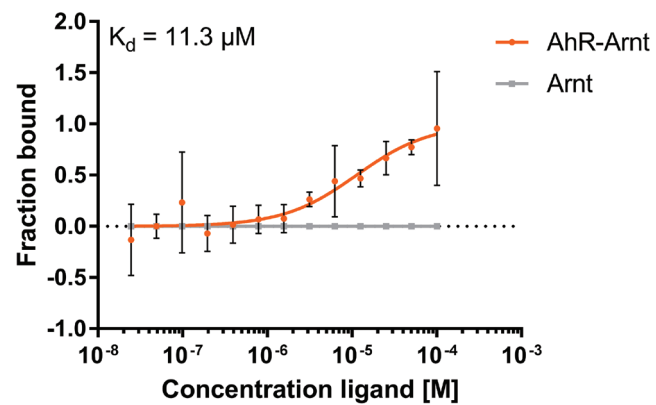
Figure 1

Figure 2

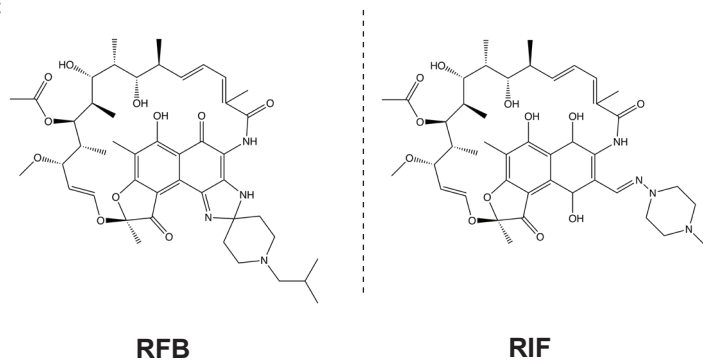
RFB



RIF



C



D

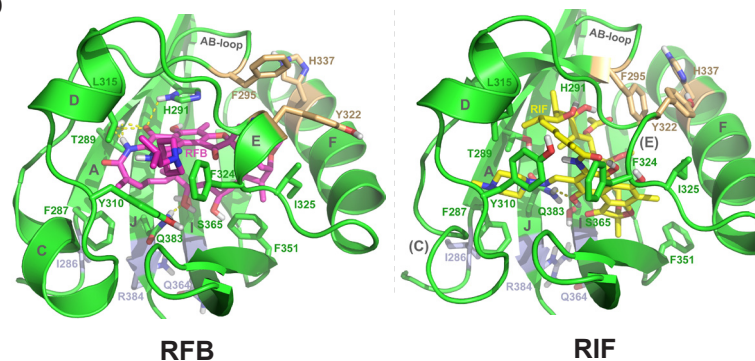
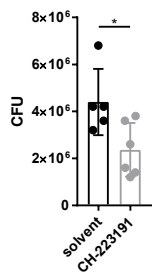


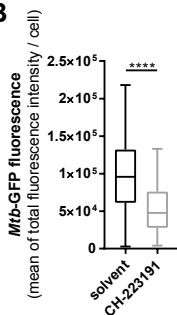
Figure 2

Figure 3

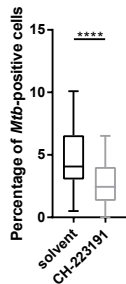
A



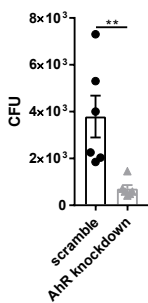
B



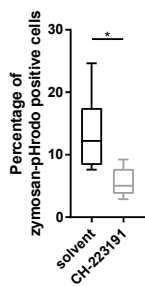
C



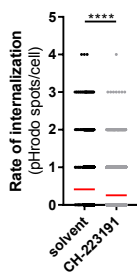
D



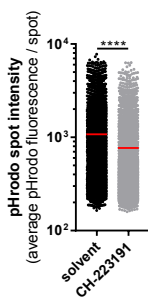
E



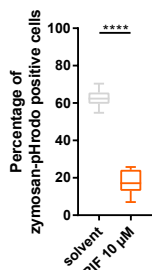
F



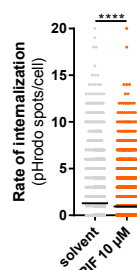
G



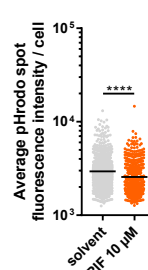
H



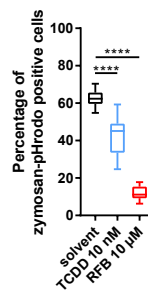
I



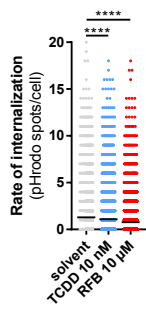
J



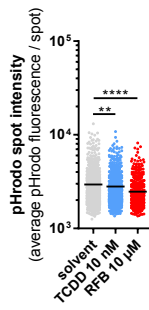
K



L



M



N

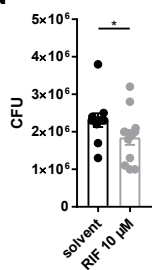
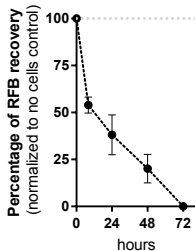


Figure 3

Figure 4

A



B

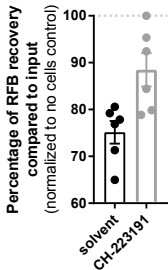


Figure 4

Figure 5

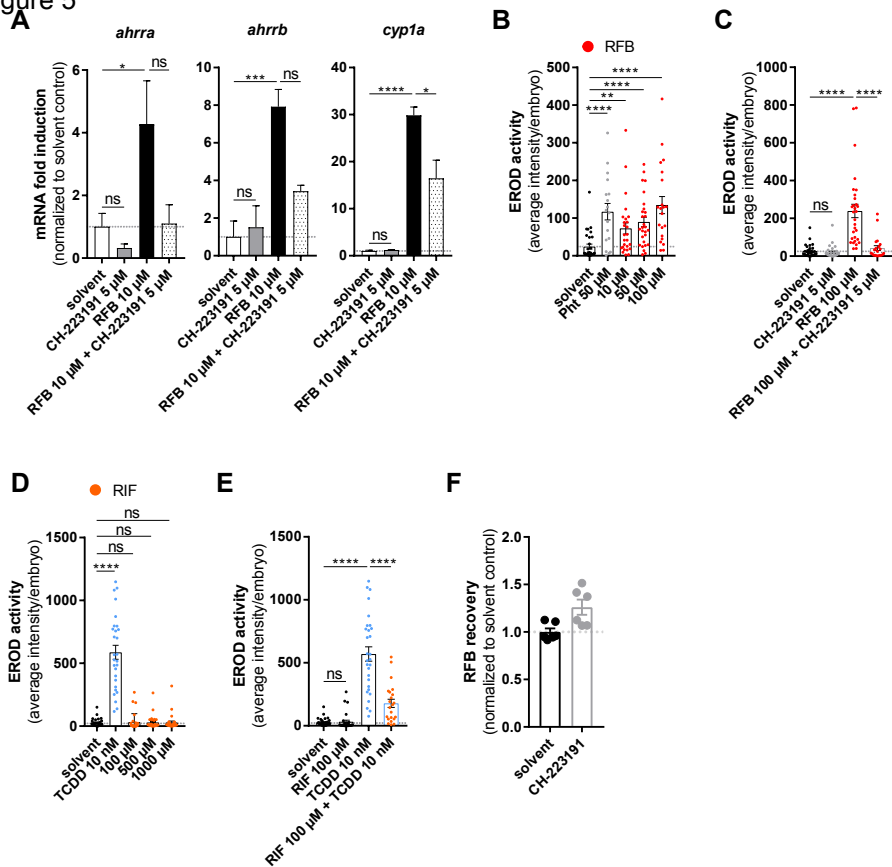


Figure 5

Figure 6

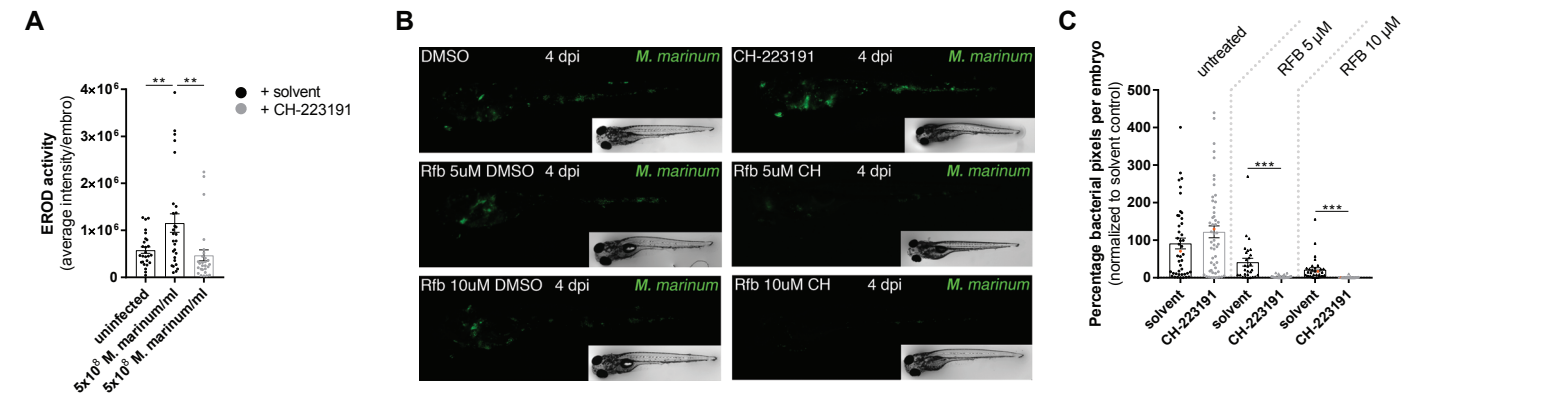


Figure 6



Click here to access/download
Supplemental Text and Figures
Supplemental_Information.pdf

